UNIVERSITÀ POLITECNICA DELLE MARCHE

FACOLTÀ DI INGEGNERIA

Dipartimento di Scienze e Ingegneria della Materia, dell'Ambiente ed Urbanistica (SIMAU)

Master Degree in **Environmental Engineering**

Comparison of UV based AOPs using mercury lamp and LED diode as irradiation source: kinetic tests with spectroscopic parameters using different radical promoter agents

Supervisor

Prof. Ing. **Francesco Fatone**

Student

Reza Abbasi

Co-supervisors

Ing. **Massimiliano Sgroi**

Ing. **Cecilia Bruni**

A.Y. **2021** / **2022**

ABSTRACT

Aim of this study was to investigate and compare the production of radical species by two UV based Advanced Oxidation Processes using two different irradiation sources: a traditional mercury lamp and innovative LED diode. Production of radical species was evaluated by using UV absorbance and fluorescence measurements, which have been shown to be very effective parameters for online monitoring of very different wastewater treatment processes. In details, investigations were performed using wastewater effluents after filtration at 0.45 μm. The AOP technology applied were UV/H2O2 and UV/Cl2. Hydrogen peroxide was used in two different dosage (30 mg/L, 50 mg/L) and Chlorine in one dosage (5 mg/L). Results were analyzed monitoring three main parameters coming from Fluorescence (fluorescence indices at defined excitation/emission wavelengths: I3(245/440 nm), I4(275/345 nm) and I5(345/440 nm)) and UV absorbance at 254 nm (UV_{254}) to have an understanding about the rate constant, degradation and also the electrical energy consumption. After carrying out all the experiments, results showed the lowest electrical energy consumption with highest reduction of fluorescence and UV254 signals when using 5 mg/L of Chlorine coupled with UV-LED instrument. In general, in terms of spectroscopic parameters removal, UV-LED lamp was more effective with Cl2, while with H2O2 mercury lamp allowed to reach higher degradation rate at the tested concentration of radical promoters (i.e.; H_2O_2 and Cl_2). In terms of energy consumption LED lamp showed better results with lower consumptions when using chlorine as radical promoter. It has been concluded that the following research gaps need to be filled: optimization of radical promoter concentration to increase degradation kinetics and reduce energy costs, and testing of additional radical promoter such as sodium persulfate.

Index

Figure Index

Table index

1. Introduction

Due to lack of efficient techniques, inappropriate disposal in water bodies and incomplete elimination from wastewater treatment plants (WWTP), variety of pharmaceuticals have been detected in the wasteway (Zhang et al., 2008). The traditional and conventional methods used to treat the wastewater are effective to some extent. They are used till today to remove the majority portion of pollutants present in the effluent. But the rising water scarcity led to necessity of reusing water and the primary and secondary treatments were not effective enough to increase the standard of reusable water that can be used for domestic and industrial purposes. Hence advanced treatment methods were found which can be introduced post the secondary treatment that aids in removing further the organic contaminants toxic materials or other nutrients present in small concentrations (Saravanan et al, 2022). At present, micropollutants such as residues from pharmaceuticals and cosmetics are frequently found in all our water bodies and have a detrimental effect on nature (https://ec.europa.eu/commission/presscorner/detail/en/qanda_22_6281). For this reason, the current revision of the Urban Wastewater Treatment Directive is addressing also these new pollutants that have emerged such as micro-plastics or micro-pollutants, which can be harmful for the environment or public health already at very low level of concentration (EU, 2022).

Nowadays, UV-based AOP has received extensive attention from scholars due to its high efficiency in dealing with problems and challenges of the removal of emerging pollutants in water. Advanced oxidation technologies (AOTs), which involve the in situ generation of highly potent chemical oxidants, such as the hydroxyl radical (•OH), have emerged as an important class of technologies for accelerating the oxidation (and hence contaminant removal) of a wide range of organic contaminants in polluted water and air. A partial list of technologies to address the issues are as followed:

- Homogeneous Ultraviolet irradiation (either direct irradiation of the contaminant or photolytic oxidation mediated by hydrogen peroxide (UV/H_2O_2), and/or ozone ($UV/H_2O_2/O_3$ or UV/O_3);
- Heterogeneous photocatalysis using semiconductor catalysts (e.g., UV/TiO_2)
- Electron-beam irradiation;
- X-ray or gamma-ray radiolysis;
- Nonthermal electric discharge;
- Supercritical water oxidation;
- Ultrasonic irradiation (sonolysis):
- Electrohydraulic cavitation.

These technologies involve widely different methods of activation, as well as oxidant generation, and can potentially utilize a number of different mechanisms for organic contaminant removal. Most of

these processes, however, are electric-energy-driven and share the common denominator of hydroxyl radical chemistry for part of the contaminant removal. Of the above AOTs, the photochemical processes are the most important commercially.

In this context, the main objective of the study is to introduce and compare conventional and innovative technologies to carry on with the removal of TOrc. Particularly, high interest in research and technological development is the implementation of new AOP technologies able to remove emerging contaminants when using reduced amount of energy.

Hence, objectives of this work were:

- To compare the degradation kinetics that describe reduction of spectroscopic parameters by two UV based technologies that used mercury lamp and LED diode as irradiation source and Cl2 and H2O2 as radical promoter
- To perform an estimation of energy consumption between the different AOPs tested in the study at laboratory scale

The work was organized in this way. First chapter of this study includes introduction and discussion of the AOP technology based on scientific literature analysis. The second chapter discusses the use of spectroscopic parameters to monitor and evaluate the Radical species coupled with the UV-Dose. After introducing the main existing technologies for irradiation, and also to produce Radical species the technology to process the irradiated effluent of wastewater to obtain and monitor the spectroscopic parameters is carried out with two different devices, one for excitation-emission and one for monitoring the UV-Absorbance, the data obtained by these two instruments would be elaborated by means of the used material and methods such as Actinometry test which helped us for the identification of all required parameters. Chapter regarding the Material and method explores the entire experimental activities performed, regarding the use of two UV equipment, one with traditional mercury lamp and one with UV-LED. Both UV have been coupled with different concentration of the two oxidants H2O2 and Cl2. In the last chapter, finally, results are reported and discussed. After carrying out all the elaborations for both chemicals used (Hydrogen-peroxide and Chlorine) data would be compared to give us a vison regarding functionality of conventional systems as opposed to UV-LED technologies.

2. AOPs technologies to remove emerging contaminants

Different AOPs such as photocatalysis, Fenton-like processes and ozonation were investigated for the treatment of an integrated solution of produced water that contains toluene, xylene, naphthalene, phenol, malonic and acetic acids. This integrated solution of produced water was referred as a seawater matrix. The efficiency in terms of total organic carbon (TOC) was studied. Among different applied AOPs, photocatalysis was less efficient for the treatment of a seawater matrix. The removals of TOC lower than 20% were noticed in 4 h of treatment. The better results were obtained in the ozonation process that combined with oxidant hydrogen peroxide (H2O2). The combined effect of H2O2 and ozone leads to the complete removal of organics, consisting of a high-percentage removal of acetic acid that was not entirely oxidized with the rest of AOPs used. 74% TOC removal efficiency was observed in ozonation for the optimum conditions of 4 g/h ozone, 500 mg/L H2O2 and pH of 10 in 2 h of treatment time. Several AOPs such as O3, O3/H2O2, UV, UV/O3, UV/H2O2, O3/UV/H2O2, Fe2+/H2O2 and photocatalysis processes were investigated for the oxidation of phenol in aqueous medium.

The comparison of these different AOPs was undertaken considering some of the experimental parameters. Among all, the Fenton process showed the fastest removal rate for phenol in wastewater. The lower costs were observed for ozonation. Single ozonation provides the best results for phenol degradation in ozone combinations. The viability of the ozonation and ozone combined with UV photolysis processes was investigated for the degradation of direct blue 86 dye in wastewater. The batch experiments were conducted for studying the effect of solution pH, initial dye concentration and reaction time. The obtained results show that the pH and initial dye concentration controls the efficiency of the process. More than 98% decolorization efficiency was obtained at pH 11, 100 mg/L of initial dye concentration in 35 min of ozone treatment. All AOPs are characterized by their potential of exploiting the higher reactivity of hydroxyl radicals while driving in oxidation processes. The different AOPs with their essential features are discussed and presented for the wastewater remediation. The number of investigations was carried out with the Fenton process for the abatement of organic pollutants in wastewater. Fenton's reagent can destroy the toxic contaminants in the wastewater like phenols and pesticides. The use of Fenton's reagent for the oxidation purpose is an attractive option for the wastewater treatment due to the iron abundances, and hydrogen peroxide is more comfortable to handle and environmentally safe. Sometimes, UV irradiation is also used with the Fenton process to increase the process efficiency. This process can overcome the shortcomings of the Fenton process.

Advanced oxidation processes differ from the other advanced treatment processes discussed (such as adsorption, ion exchange, or stripping) because organic compounds in water are degraded rather than

concentrated or transferred into a different phase. Further, compounds that are not adsorbable or only partially adsorbable may be destroyed by reaction with hydroxyl radical. Because a secondary waste stream is not generated, there is no additional cost to dispose of or regenerate materials. Hydroxyl radicals are capable of oxidizing almost all reduced materials present without restriction to specific classes or groups of compounds, as compared to other oxidants. In addition to being non-selective, many AOPs operate at normal temperature and pressures. Other processes that can generate hydroxyl radicals, but require elevated temperature and/or pressure, include catalytic oxidation, gas-phase combustion, supercritical oxidation, and wet oxidation processes. Several technologies are available to produce • OH in the aqueous phase (U.S. EPA, 1998). Selected technologies are summarized in Table below (Table 1). While in Figure 1, Figure 2 and Figure 3 are reported some example from literature of AOP scheme and reactors.

Table 1: General technologies of AOP (Metcalf & Eddy)

Advanced oxidation process	Advantages	Disadvantages
Hydrogen peroxide/ ultraviolet light	H2O2 is fairly stable and can be stored on site temporarily prior to use	H_2O_2 has poor UV absorption characteristics and if the water matrix absorbs UV light energy then most of the light input to the reactor will be wasted Special reactors which are designed for UV illumination are required Residual H_2O_2 must be removed Potential for UV lamp fouling
Hydrogen peroxide/ ozone	Waters with poor UV-light transmission may be treated Special reactors designed for UV illumination are not required Volatile organics will be stripped from the ozone contactor (VOCs may require treatment)	Production of O_3can be an expensive and inefficient process Gaseous ozone which is present in the off gas of the ozone contactor must be removed Maintaining and determining the proper O_3/ H_2O_2 dosages may be difficult
Ozone/UV	No need to maintain precise dosages of O3/H2O2 Residual oxidant will degrade rapidly (typical half-life of O3 is 7 minutes) Ozone absorbs more UV light than an equivalent dosage of hydrogen peroxide. (~200 times more at 254 nm) Volatile compounds will	Must use O_3 and UV light to produce H2O2, which is the primary means of producing • OH and using O_3 to produce H2O2 is very inefficient as compared to just adding H2O2 Special reactors which are designed for UV illumination are required Ozone in the off-gas must

	be stripped from the process (VOCs may require treatment)	be removed Potential for UV lamp fouling
Ozone/UV/H_2O_2	Commercial processes that utilize the technology are available H2O2 promotes ozone mass transfer Volatile compounds will be stripped from the process. (VOCs may require treatment)	Special reactors that are designed for UV illumination are required Ozone in the off-gas must be removed Potential for UV lamp fouling
Fenton's reactions (Fe/ hydrogen peroxide, photo-Fenton's or Fe/ ozone	Some effluents may contain sufficient Fe to drive the Fenton's reaction Commercial processes are available that utilize the technology	Process requires low pH
Titanium dioxide/UV	Activated with near UV light; consequently greater light transmission is achievable	Fouling of the catalyst may occur When used as a slurry, the TiO_2 must be recovered Potential for UV lamp fouling
Ozone at elevated pH (8 to .10)	Does not require the addition of UV light or hydrogen peroxide	Ozone is the off-gas must be removed pH adjustment is not practical in most wastewater applications There are no commercial applications Process does not yield an appreciable destruction for contaminants

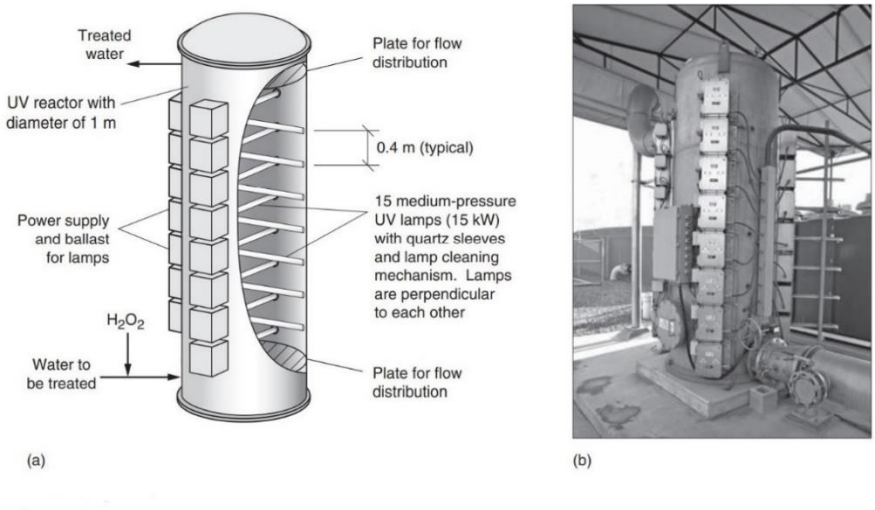

Hydrogen peroxide and UV radiation advanced oxidation process (a) schematic diagram (from Crittenden et al., 2012) and (b) photograph of typical vertical flow UV reactor.

Figure 1: UV/H_2O_2 typical reactor

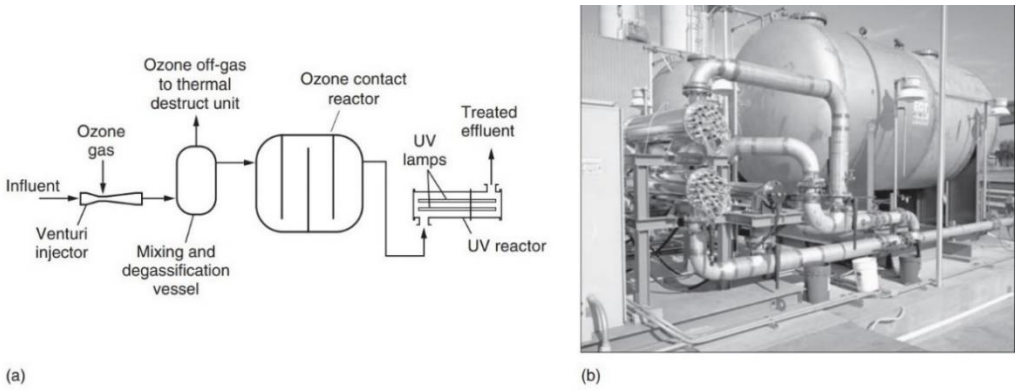

Advanced oxidation process involving the use of ozone and UV radiation (a) schematic representation (ozone contactor shown without chimneys, (b) view of full scale installation.

Figure 2: UV/O_3 general Scheme

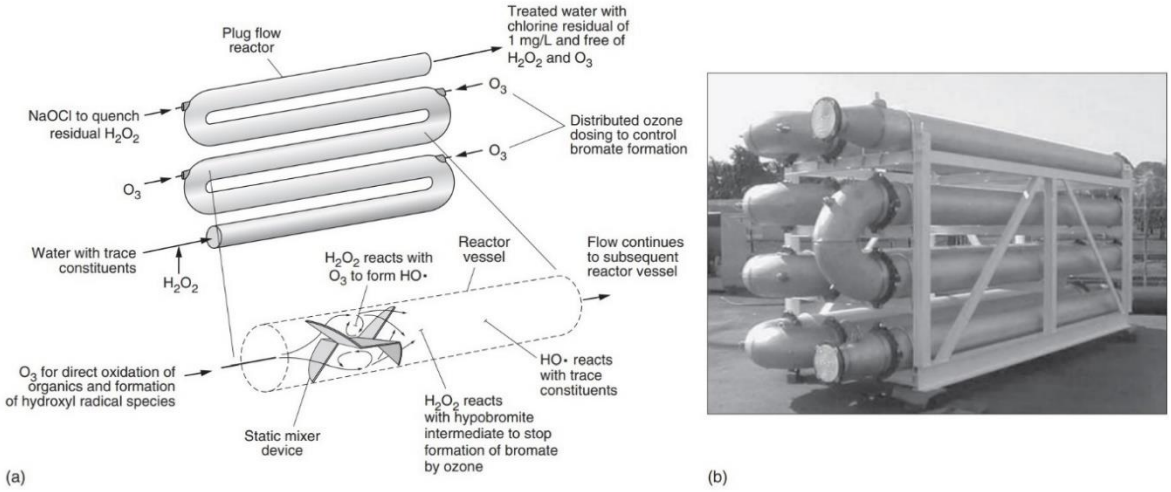

Advanced oxidation process involving the use of ozone and hydrogen peroxide (a) schematic of HiPOx® reactor and (b) view of reactor described in (a) (courtesy of Applied Process Technology, Inc., Pleasant Hill, CA.).

Figure 3: O_3/H_2O_2/UV general scheme

Photolysis is a process by which constituents are broken down by exposure and absorption of photons from a light source. As with AOPs, the primary use of photolysis is for the removal of trace organic compounds in water reuse applications. In natural systems, sunlight is the light source for photolysis reactions, however, in engineered systems, ultraviolet (UV) lamps are used to produce the photonic energy. The photons that are absorbed cause the electrons in the outer orbital of some compounds to become unstable and split or become reactive. The effectiveness of the photolysis process depends, in part, on the characteristics of the reclaimed water, structure of the compounds, design of the photolysis reactor, and dose and wavelength of the applied light. The photolysis rate can be estimated from the rate at which the compound absorbs light and the photonic efficiency of the reaction (quantum yield). Photolysis may be used for the removal of various compounds, such as NDMA and

other trace organic constituents. It should be noted that many compounds are not removed using photolysis alone, and that the addition of hydrogen peroxide can enhance the degradation of these constituents. However, the addition of hydrogen peroxide may actually reduce the photolysis of some compounds, such as NDMA (Linden et al., 2004).

The UV spectral range of interest in UV light-based water treatment for environmental contaminant and microbial pathogen removal is the UV-C region (200–280 nm), where many chemical compounds, DNA and hydrogen peroxide absorb the UV radiation. Particular AOP applications use the vacuum UV range (VUV, 100–200 nm) in which water is the main light absorber. In principle, any radiation carrying energy equal or higher than the chemical **bond dissociation energy** (BDE, $\Delta E°$, J mol^{-1}) can break the respective bond. The probability of such process to occur depends on two factors:

1. the strength of light absorption, which is described by the optical properties of chemical compound,
2. the probability of the excited state generated through the light absorption event to undergo a chemical reaction.

The descriptors of these two factors are the **molar absorption** coefficient and the **quantum yield**. For a given, well-characterized light source, the development of a kinetic model for predicting the UV/H_2O_2, process performance requires good understanding of direct photolysis, radical generation and radical reaction mechanisms involving target compound(s), H_2O_2, and at least the key water matrix constituents namely the dissolved organic matter, nitrate, and carbonate species, as well as the pH and water absorption impact. As not all radical reactions occurring in a UV/ H_2O_2, –based water treatment contribute significantly to the process performance, usually, sensitivity analyses are performed and the kinetic model is constructed based on relevant reactions and equations.

The latest advancements in semiconductor technology have led to the development of light emitting diodes (LEDs) capable of emitting a narrow spectrum of UV radiation (UV LEDs) at wavelengths capable of inactivating pathogenic organisms. Recently, UV LED chips and packages, as the primary products, have been evolving in terms of power output, lifetime and even production cost management. Recent advances in UV LED technology have now made it possible to apply this technology to water treatment. In fact, UV LED possesses attractive features that can bring innovations to UV technologies for water treatment. Here, three important aspects of UV LED water treatment systems are discussed: design, operation and application. The UV lamps designed for water treatment (disinfection and AOPs) have significant output in the 200–300 nm wavelength range. The Hg vapor-based lamps contain Hg in its physical state (liquid) or in amalgams and a rare gas (argon,

neon, xenon, helium), most commonly argon (Ar). Mercury has relatively high vapor pressure and low ionization energy, is quasi-chemically inert toward the quartz and electrode materials, and its resonance lines are in the UV range. The lamp assembly has a few components and the lamps come in various lengths and tube diameters. The artificial light sources emit either monochromatic or polychromatic radiation of wavelengths determined by the nature of the emitting atoms or molecules, concentration and energy of the excited states, and the probability of the radiative transitions. The wavelength, sharpness, and relative intensity of the emitted lines depend on the pressure of both Hg and rare gas. The source of energy for most light sources is electricity, and the excited states are mostly generated via collisions with highly energetic electrons, accelerated in the electric field. Grotian energy level diagram for mercury atoms in their ground and excited states (singlet and triplet states) illustrates the radiative transitions between Hg energy levels and helps the reader understand the origin of Hg lines in mercury-vapor lamps. The resonance lines of Hg atoms are at 184.9 nm and 253.7 nm. Upper excited states of Hg can be reached and radiative emissions from those states occur depending on the Hg vapor pressure. (Stefania Mihaela I.,2018).

Recently, the UV/Chlorine process has been investigated as an alternative to the UV/H2O2 process and was tested at a few water treatment utilities (pilot- or full-scale) for water reuse, drinking water production, or groundwater decontamination. As mentioned by Allmand et al. (1925), the photodecomposition of chlorine in water has been investigated since the 1850s. Buxton and Subhani (1972b) showed that the photodecomposition mechanism of hypochlorite ion is very complex and depends on the irradiation wavelength. Photodecomposition of hypochlorite ion leads to chloride, chlorate, chlorite, and oxygen as end-products and to the in situ generation of •OH and Cl• as well as many other unstable intermediates. A few research works performed in the 1970s showed that UV/Cl2 can oxidize or mineralize completely organic compounds which are resistant to chlorine in the dark and to direct photolysis. These reactions have been demonstrated in the case of ethanol, n-butanol and benzoic acid at pH < 10 and at ~350 nm (Oliver & Carey, 1977), ethylene glycol dimethyl ether and related substrates, acetic and propionic acids at pH > 12 with a high pressure Hg lamp (Ogata et al. 1978; Ogata et al. 1979), benzoic acid at pH ≥ 12 and $\lambda = 253.7$ nm and $\lambda \geq 350$ nm (Ogata & Tomizawa, 1984), benzoic acid and nitrobenzene at pH 6 and $\lambda \geq 350$ nm (Nowell & Crosby, 1985), 1-chlorobutane, n-octanol and nitrobenzene at sunlight wavelengths (Nowell & Hoigné, 1992b).

Absorption spectra of free chlorine species in water is shown in the Figure 4.

1 $Cl_2 + H_2O \rightleftharpoons HOCl + H^+ + Cl^-$ $K_d = 3.94 \times 10^{-4}$ M^2 at 25°C and $I = 0$

2 $HOCl \rightleftharpoons ClO^- + H^+$ $pK_a = 7.537$ at 25°C and $I = 0$ (Morris, 1966)

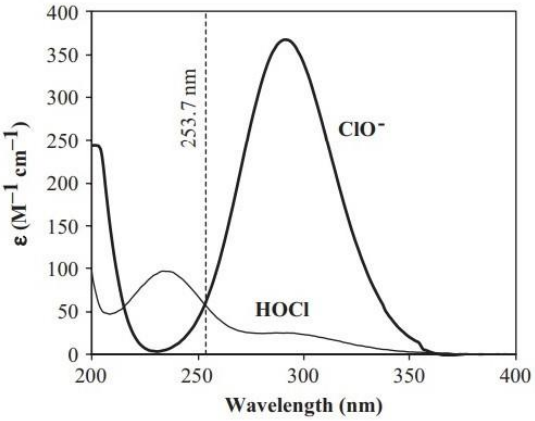

Figure 4: Absorption spectra of free chlorine species in water

HOCl and ClO− absorb UV light at wavelengths ranging from 200 to 375 nm and therefore, free chlorine can be photolyzed by UV-C light, as well as by the UV-B and UV-A radiation from the solar light (Buxton & Subhani, 1972b; Nowell & Hoigné, 1992a). Molar absorption coefficients (ε) range from 0 to 370 M−1 cm. Absorption spectra show a maximum absorption band centered at 236 nm for HOCl.

From steady-state and flash photolysis experiments on sodium hypochlorite solutions at alkaline pH, Buxton and Subhani (1972b) showed that the primary photoproducts of hypochlorite ion as well as the primary quantum yields of photoproduct formation depend on the irradiation wavelength. The primary products of photolysis of hypochlorite ion are chloride ion, hydroxyl radicals (•OH/O•−, pKa = 11.9; Buxton et al. 1988), Cl• and O(3P) at 253.7, 313 and 365 nm. O(1D) is also produced at 253.7 nm and 313 nm. The quantum yields of formation of (•OH/O•−) and Cl• from ClO− photolysis markedly decrease when irradiation wavelength increases, e.g., from 0.28 at 253.7 nm to 0.08 at 365 nm. Similarly, •OH, Cl• and oxygen atoms are formed by UV photolysis of HOCl (Kläning et al. 1984; Thomsen et al. 2001; Herrmann, 2007). Cl• exhibits a strong absorption band in the UV region with a maximum at around 310–320 nm (Figure 5) (Kläning & Wolff, 1985; Buxton et al. 2000; Thomsen et al. 2001). From femtosecond photolysis experiments of HOCl (~1.5 M) at 266 nm, Thomsen et al. (2001) showed that HOCl molecules photo dissociate within 1 picosecond into •OH and Cl• with a near-unity quantum yield.

$$HOCl \xrightarrow{h\nu} {}^{\bullet}OH + Cl^{\bullet}$$

$$Cl^{\bullet} + HOCl \rightarrow Cl_2 + {}^{\bullet}OH$$

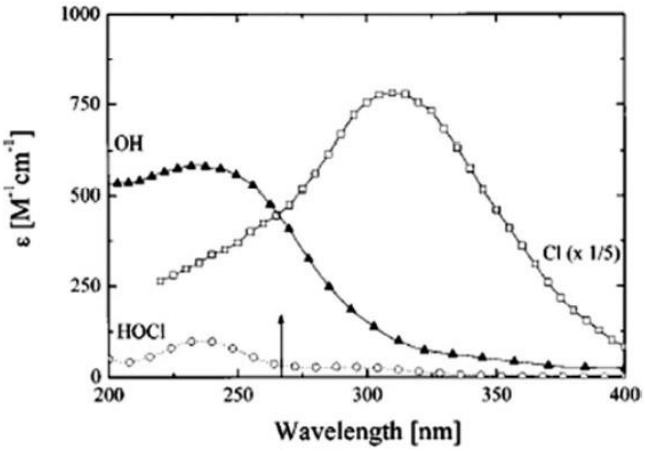

Figure 5: Absorption spectra of HOCl, •OH and Cl•

Hydrogen peroxide is a weak absorber of UV radiation. The molar absorption coefficients of H H_2O_2 and of its conjugate base, hydroperoxide ion HO_2^- (pKa = 11.7) in aqueous solution are available in the published literature. The molar absorption coefficients of HO_2^- are larger than those of H_2O_2; e.g., ε(H_2O_2, 210 nm) = 189 ± 28 M^{-1} cm^{-1} , ε(HO2 −, 210 nm) = 733.7 ± 63.1 M^{-1} cm^{-1}; ε(H H_2O_2, 300 nm) = 0.96 ± 0.21 M^{-1} cm^{-1}; ε(HO_2^-, 300 nm) = 27.3 ± 1.0 M^{-1} cm^{-1} (Morgan et al. 1988). At 254 nm, ε(H_2O_2) is ~19.2 M^{-1} cm^{-1}. Chu and Anastasio (2005) reported the molar absorption coefficients of H_2O_2 (6.5–26 mM) as a function of wavelength (240–380 nm) and temperature (1–25°C). A steady yet small increase was observed at 25°C relative to 1°C, e.g., from 0.5% at 240 nm to ~6.6% at 280 nm, with 2.2% increase at 254 nm. Given the poor UV light absorption properties of H_2O_2 relative to those of water matrix constituents, H_2O_2 must be properly dosed in the UV/ H_2O_2 applications such that the amount of UV light absorbed by H_2O_2 generates the • OH yield required for meeting the process performance. The optimum H_2O_2 dose is application-specific and depends on several factors among *which water quality, lamp type and power, reactor design, contaminant reactivity toward • OH, contaminant treatment level, and direct photolysis* contribution to the overall treatment. In typical surface water and groundwater, only a small fraction of UV radiation emitted by the light source is utilized to produce • OH, and small reductions (up to ~15%) in H_2O_2 concentrations are observed.

Hydroxyl radical properties, and quantification in aqueous solutions:

Hydroxyl radical is a neutral free radical and one of the most powerful oxidizing radical species. The most important properties of • OH directly related to its chemical reactivity are the reduction potential E_o (pH-dependent; 2.7 V and 1.8 V in acidic and alkaline media, respectively), pK_a (~11.9) and diffusion coefficient (2.3 × 10^{-5} cm^{-2} s^{-1}) (Dorfman & Adams, 1973). In its reactions with organic compounds, • OH behaves as an electrophile, attacking the electron-rich sites of molecules, whereas its conjugate base • O− is a nucleophile. As a powerful oxidizing species, • OH attacks the organic

and inorganic compounds non-selectively, and most of its reactions approach the diffusion-controlled limits. The high reactivity of • OH explains its very low steady-state concentrations (10^{-10}– 10^{-12} M) in water. The rate constants of • OH reactions with organic compounds of environmental interest range from ~106 to 1010 M^{-1} s^{-1} . The • OH reactions with chemical compounds include hydrogen atom abstraction, addition to electron-rich sites such as unsaturated bonds and aromatic rings, and electron-transfer. Chemical probes with well-known rate constants and product yields for the reaction with • OH were used with both pulse radiolysis and steady-state irradiation techniques to quantify • OH yields. Chemical compounds used as probes for • OH quantification include salicylic acid, p-hydroxybenzoic acid, methanol, dimethyl sulfoxide, terephthalate, dihydroxybenzoate, coumarin-3-carboxylic acid, 3′-p-(amino phenyl)fluorescein. The products from these probes can be analyzed by commonly used analytical methods such as HPLC with UV or electrochemical detection, derivatization followed by UV-Vis spectroscopy, FLUORESCENCE spectroscopy, GC/MS. The probe selection, • OH generation method, matrix, analytical method, as well as other factors which can influence the accuracy of the experimental outcomes must be carefully considered.

2.1 UV AOPs technologies with standard Hg lamp

The standard LP Hg lamp operates in either arc (‘hot’ cathode) or glow discharge mode (‘cold’ cathode). The filling is a mixture of mercury and an inert gas, typically argon. The lamp is operated at ~40–42°C and the Hg vapor pressure is 1–10 mbar. The role of argon is to initiate and maintain the discharge, to reduce the required starting voltage for discharge, to act as a buffer protecting the electrodes from sputtering and evaporation, thus extending the lamp lifetime. When the lamp is switched on, the electrons are accelerated in the electric field. The collisions between the energized electrons and atoms are elastic and result in energy transfer with the generation of excited states of the atoms (Hg* and Ar*). The radiative deactivation of Hg* states to the ground state in LP lamps result in the resonance mercury lines of 253.7 and 184.9 nm. Radiative transitions from the upper excited states of the Hg atoms also occur, but their intensities are very low as compared to the 253.7 nm line, given the low populations of those excited states.

The radiant power efficiency at 253.7 nm of current commercial LP Hg lamps can be up to ~40%. The output depends on the operating temperature. The concentration of Hg atoms in the discharge must be controlled in order to obtain the maximum UV-C output from the input electrical energy. The optimum pressure is approx. 0.006 torr (Light Sources Inc, 2013). A better version of standard LP lamp is the LP high-output (LPHO) lamp, whose electrode assembly has a “dead” volume behind the filaments (“cold spot temperature region”) which needs to be held at ~40°C in order to achieve optimum efficiency at 253.7 nm. The lamp can be operated at wall temperatures higher than 50°C, and the specific lineal power per arc length (mW/cm) is higher than that of standard LP lamps (Schalk

et al. 2006). The impact of ambient temperature on lamp efficiency was overcome by introducing the LP amalgam lamps, in which Hg is introduced as amalgams with bismuth, indium, or gallium – typically with indium. The "long life technology" based on effective coatings developed by Voronov et al. (2003) ensures more than 90% of the initial UV-C output over >16,000 h of lamp operation. compares the key features of various LP lamps in the Table 2 and Figure 6 we could observe the general spectral distribution of the radiation for different mercury lamp's technologies with their electrical power consumption .

Table 2: General characteristics of UV-Mercury lamps

Characteristics of commercial LP Hg-vapor arc lamps; adapted from Schalk *et al.* (2006) and Light Sources Inc (2013).

Feature	TiO_2 Doped Doped Quartz, Soft Glass	Natural or Synthetic Fused Quartz		Natural or Synthetic Fused Quartz Amalgam Lamp
		Standard	High Output	
Emitted radiation	253.7 nm	184.9 nm, 253.7 nm	184.9 nm, 253.7 nm	184.9 nm, 253.7 nm
Wall temp. (°C)	30–50	30–50	>50, cold spot 40	90–200
Current (A)	0.2–0.5	0.3–0.4	0.8–1.3	1.2–5.0
Arc length (cm)	7–148	5–155	27–200	27–200
Electrical power (W)	5–80	5–80	10–150	40–1000
Specific electrical power* (W/cm)	0.25–0.3	0.3–0.5	0.5–1.0	1.0–5.0
Specific UV-C radiant power* (mW/cm)	<175	<200	<350	<2000
UV-C (253.7 nm) efficiency (%)	25–35	30–40	25–35	30–38
Lifetime (h) for >90% initial 253.7 nm output	9000 (>85%)	16,000 (>85%)	12,000	16,000

*per unit of arc length.

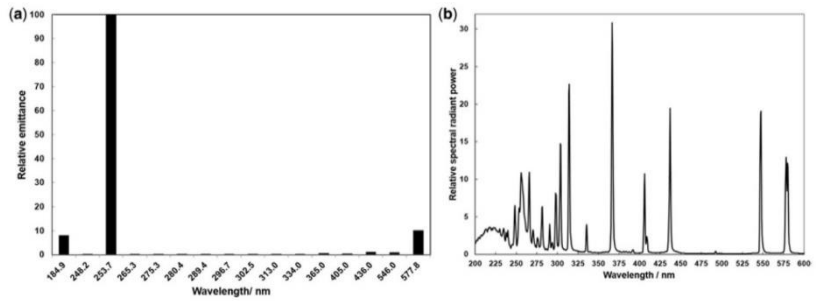

Relative spectral distribution of the radiation emitted from (a) LP and (b) MP Hg vapor arc lamps (Stefan, 2004).

Figure 6: Low Pressure and Medium pressure distributions of radiation lamp

2.2 UV-LED AOPs technologies

The general trend in science and technology towards the development and implementation of environmentally friendly "green" processes has prompted numerous research studies on Hg-free lamps for water disinfection and contaminant removal. Excimers, Hg-free flash lamps and light emitting diode (LED)-based UV light sources were developed for UV applications. Despite the progress achieved on their technology, these lamps have not reached the overall performance of LP– and MP– Hg vapor arc lamps and are not used in full-scale installations for water treatment.

2.2.1: Excilamps

The non-coherent excimer and exciplex lamps are gas-discharge quasi-monochromatic light sources. The electromagnetic radiation is produced by either microwave discharges or 'silent' electrical discharges (also called dielectric barrier discharge, DBD) in the same gas or mixture of two gases. The emission spectrum depends on the nature of the fill gas. These light sources operate near room temperature, do not emit IR radiation, and the electric discharge requires high voltages (up to 20 kV) and high frequency ranges (kHz to MHz). The fill gas in these lamps is either a noble gas (Ne, Ar, Kr, Xe) which case, the excited state (e.g., Xe2*) emitting the radiation is called excimer, or mixtures of a noble gas and a halogen, in which case the excited state (e.g., XeCl*) is called exciplex.

The exclaims present several advantages over the Hg-vapor lamps, including: flexible design geometry, no warmup time, long lifetime (up to 10,000 h depending on design and operating conditions), electrodeless, narrowband emission, high photon flux without absorption of emitted radiation, V/VUV power efficiency from 1–2 to 60% depending on the fill gas, near room temperature operation, Hg-free, thus, environmentally friendly light sources (Sosnin et al. 2006). Spectral emission of excimers and exciplexes, characteristics of excilamps and their limitations, recent advancements in their construction and power supplies, as well as references to the studies in this field are provided in Chapter 5 of this book. Most studies on exciplex lamp applications were in the VUV region and concerned primarily the mineralization of organic compounds. Recently, Matafonova and Batoev (2012) reviewed the research studies on UV radiation from excilamps for contaminant treatment in water by direct photolysis and AOPs, and as a pre-treatment step in combination with biodegradation.

2.2.2: Pulsed UV lamps:

Pulsed light technology is based on pulsed electrical energy discharges in inert gases (Xe, Ar, Kr). The pulse duration is generally between 50 and 3000 microseconds, and the interval between pulses is in the order of milliseconds. The electrical discharge heats the fill gas (typically Xe) almost instantly to very high temperatures (≥13,000 K) that compresses in a thin 'shell' of plasma (ionized gas, electrons, excited states) on the inner wall of quartz envelope. The heated plasma emits blackbody continuum radiation characteristic to plasma temperature. The shape of spectral emission in the UV range is also plasma temperature-specific, thus, is determined by the flash lamp operating conditions. Approx. 38–52% of total radiative output can be reached within the 185–400 nm range with an average UV-C efficiency of 15–20% (Haag, 1994). Xenon is the preferred rare gas given its low ionization potential (Eo = 12.1 eV; Masschelein, 2000), despite being more expensive than Ar and Kr. The radiation emitted by the plasma is not absorbed by the rare gas. The UV fluence rates from these lamps can be three to four orders of magnitude higher than those from Hg-vapor arc lamps.

The characteristics of radiation emitted from pulsed light sources are described in the literature (Phillips, 1983; Marshak, 1984; Haag, 1994; Schaefer et al. 2007). An approach to the standardization of fluence determination in bench-scale pulsed light experiments was recently described by Gómez-López and Bolton (2016). The pulsed UV lamps reach the full-power instantly, and their spectral UV radiation output is driven by the lamp and power supply settings. The excessively high pulse energies (applied voltage as high as 30 kV) increase thermal stresses which shorten drastically the lamp lifetime. Pulsed UV lamps were successfully tested at laboratory scale for both pathogen inactivation and environmental contaminant removal in water. High removal yields in short exposure times were achieved for several water contaminants, among which, NDMA (Liang et al. 2003), chlorinated aliphatic compounds (Haag, 1994), pesticides (Baranda et al. 2014)

2.2.3 Light-emitting diode (LED) lamps:

LED-based light sources have been successfully commercialized for more than five decades (since 1962) for indoor and outdoor lighting and are largely used in analytical instrumentation. LEDs convert the electrical energy to radiation via electron-hole recombination at the p-n junction in the semiconductor chip. The e^{-}-hole (h^{+}) recombination generates a high energy state which releases a photon upon relaxation; the photon wavelength depends on the semiconductor materials used in LEDs. Electroluminescence in the UV range was reported from doped wide bandgap materials such as diamond (λ = 235 nm; Koizumi et al. 2001) and group III element nitrides (e.g., GaN, AlGaN, and AlN), with the shortest wavelength (210 nm) LED (AlN PIN (p-type/intrinsic/n-type) developed and characterized by Tanyiasu et al. (2006). UV radiation covering the 210–365 nm range can be obtained from AlGaN LEDs where AlN and GaN are combined at specific ratios. UV-C LEDs emit in all directions yet are limited by material and construction to be point source emitters. The optical power density (mW/cm2) from a 30 mW UV-C LED is approx. 1.8-fold and 50-fold higher than that from a typical MP Hg lamp and a typical LP amalgam lamp, respectively (Pagan & Lawal, 2015). Remarkable advancements were reported in UV LED manufacturing and commercialization, and the output power per single chip of commercial LEDs increased from ~2 mW in 2012 to 30 mW in 2015, with lifetimes in thousands of hours (Pagan & Lawal, 2015). LEDs can be operated in either pulsed or continuous mode. These light sources present a number of advantages over the Hg-vapor lamps: higher UV power density, are operated of direct current (D.C.), compactness, robustness, instant startup to full power, lower electrical power consumption, longer lifetime, wavelength tenability, flexible geometry and reactor design, environmentally safe. However, currently, the UV-C LEDs are cost-prohibitive, have low wall-plug efficiency and undeveloped product design. The UV-C LEDs were extensively examined for their capability to inactivate microbial pathogens in water and on surfaces (Song et al. 2016). Very limited work was reported on UV-LEDs for micropollutant removal,

most of which concerned the UV-A (365 nm) LED/TiO2 AOP. Autin et al. (2013) evaluated Al-In-Ga-nitride LEDs emitting at 255, 310 and 365 nm in combination with either TiO2 or H2O2 for methylene blue and metaldehyde (pesticide) removal in simulated surface water. In 2012 AquiSense Technologies launched the first UV-C LED product designed for low-flow water disinfection from the PearlAqua platform.the general Inactivation caused by UV-Irradiation is shown in Figure 7.

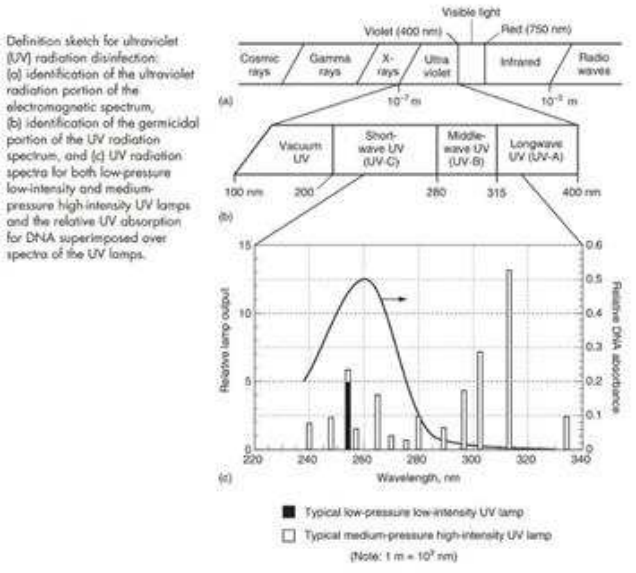

Figure 7: General Domain of UV-Radiation Inactivation

The portion of the electromagnetic spectrum in which UV radiation occurs, is between 100 and 400 nm. The UV radiation range is characterized further according to wavelength as longwave (UV-A), also known as near-ultraviolet irradiation, middle wave (UV-B), and shortwave (UV-C), also known as far UV. The germicidal portion of the UV radiation band is between about 220 and 320 nm, principally in the UV-C range. The UV wavelengths between 255 to 265 nm are considered to be most effective for microbial inactivation. Most commonly, UV radiation is produced by striking an electric arc between two electrodes in specially designed lamps containing liquid mercury, as well as other gas mixtures. The energy generated by the excitation of the liquid mercury causes it to vaporize. Mercury in its gaseous form excites electrons in the lamps thus producing photons of UV light. When used for water and wastewater effluent, quartz sleeves are most often used to isolate the UV lamps from direct water contact and to control the lamp wall temperature by buffering the effluent temperature extremes to which the UV lamps are exposed, thereby maintaining a fairly uniform UV lamp output. In another less common configuration, the water to be disinfected is passed through proprietary plastic tubes that are themselves surrounded by UV lamps. The output of UV degradation systems also decreases with time due to a reduction in the electron pool within the UV lamp,

deterioration of the electrodes, and the aging of the quartz sleeve. Lamps with other gas mixtures and without electrodes, as described below, are also used to generate UV light.

3. Use of spectroscopic parameters to monitor AOPs process

reference(https://doi.org/10.1016/j.coesh.2017.11.003)

Use of optical surrogate parameters, notably those based on absorbance and fluorescence, has been particularly important for water quality monitoring. Contributions of dissolved organic matter (DOM) or effluent organic matter (EfOM) to the absorbance of wastewater or surface water, and changes of these spectra associated with water treatment or with transformation of DOM/EfOM in natural systems are indicative of the concurrent effects on trace organic contaminants (TrOCs). That review compares the use of single-wavelength indicators (e.g., A254), combinations of absorbance measurements at up to four wavelength, ratios of absorbance at indicative wavelengths (e.g., A_{254}/A_{202}) the interpretation of absorbance data using the differential absorbance approach and processing multi-wavelength absorbance spectra in $\log^{A}$ coordinate. These and related options are compared in some details in table below:

Table 3:Absorbance-Based surrogate water parameter

Abridged list of absorbance-based surrogate water parameters for quality monitoring.

Parameter	General Interpretation
A_{254}	Standard UV absorbance parameter
A_{254}/A_{202}	Ratio of absorbance at 254 and 202 nm; a measure of activation of NOM (can be affected by the presence of nitrate)
$\frac{\Delta A_\lambda}{A_{\lambda,0}}$	Relative treatment-induced change of water absorbance at wavelength λ.
$\Delta A_\lambda = A_{\lambda,0} - A_{\lambda,treated}$	Differential change of water absorbance at wavelength λ determined vs. the absorbance prior to treatment.
S_{λ_1,λ_2}	Slope of log-transformed absorbance spectra the range of wavelength λ_1 to λ_2
$\ln\left(\frac{A_\lambda}{A_{\lambda,0}}\right)$ or $\ln\left(\frac{\Delta A_\lambda}{A_{\lambda,0}}\right)$	Logarithm of relative change of absorbance
$ASI = 0.56\frac{(A_{254}-A_{272})}{(A_{220}-A_{230})}$	Absorbance slope index; deemed to be a measure of the molecular weight of NOM and its activity

One difficulty in using absorbance spectroscopy for water quality monitoring is that the absorbance spectra of DOM/EfOM comprise contributions of multiple chromophores and inter-chromophores interactions.

Fluorescence is a measure of the intensity of energy emitted (in the UV and visible range) by excited molecules that absorbed light energy (excitation) (Mladenov et al., 2018). Several studies have demonstrated the potential of fluorescence spectroscopy for treatment process control. The technique offers practical advantages, such as: fast measurements, cost-effectiveness, lack of need for reagents, and high sensitivity (Carstea et al., 2018). In addition, fluorescence holds promise due to its ability to discriminate several classes of organic compounds and provide in situ and instantaneous measurement (Mladenov et al., 2018).

The fluorescence Excitation-emission matrixes (EEMs) of all samples were measured, these spectra are featureless although DOM/EfOM properties such as its aromaticity, apparent molecular weight can be estimated based on single-wavelength parameters (e.g., absorption coefficient at 280 nm e ε280, specific UV254 absorbance - SUVA254), absorbance ratios (e.g., A254/A202, absorbance slope index -ASI) and slopes of the log-transformed absorbance spectra.

Excitation-emission matrixes (EEM) of natural waters and wastewater tend to have distinct features with maxima located at characteristic combinations of excitation and emission wavelengths. Different methods have been developed to interpret the information in EEMs, from simple peak-picking, in which different fluorescence peaks are selected from several defined wavelength ranges of EEM to the more complex Parallel Factor Analysis (PARAFAC), which can decompose the complex fluorescence spectra into a finite number of potentially overlapping independent components characterized by their distinct spectroscopic features. The presence of various EEMs features allows tracking contributions of the indicative fluorophores groups as a function of water treatment or the presence of wastewater in an affected body of water. Table below presents an abridged list of fluorescence-based parameters whose utility in water quality monitoring has been examined in recent research.

Table 4: Fluorescence-based surrogate water parameter

Abridged list of fluorescence-based surrogate water parameters for quality monitoring.

Parameter	General Interpretation
$FI = \frac{F_{\frac{370}{450}}}{F_{\frac{370}{500}}}$	Fluorescence Index, interpreted as an indicator of aromaticity
$HIX = \frac{\left(\sum F_{\frac{254}{435}\rightarrow 480}\right)}{\left(\sum F_{\frac{254}{300}\rightarrow 345}\right)}$	Humification Index, interpreted as an extent of natural organic matter humification
$BIX = \frac{F_{\frac{310}{380}}}{F_{\frac{310}{430}}}$	Biological index, deemed a measure of DOM endogenous contribution
Peak B ($\lambda_{ex/em}$ = ~225 (~280)/~305 nm)	Proteins and tyrosine-like fluorescing substances
Peak T_1 ($\lambda_{ex/em}$ = ~225/~350 nm)	Proteins, microbial products and tryptophan-like fluorescing substances
Peak T_2 ($\lambda_{ex/em}$ = ~280/~350 nm)	Proteins, microbial products and tryptophan-like fluorescing substances
Peak A ($\lambda_{ex/em}$ = ~225/400–500 nm)	Microbial products, fulvic and humic-like fluorescing substances
Peak C ($\lambda_{ex/em}$ = 300–350/400-500 nm)	Terrestrial humic-like fluorescing substances
Peak M ($\lambda_{ex/em}$ = 310–320/380–420 nm)	Autochthonous production, marine and terrestrial humic-like fluorescing substances
$\frac{\text{Peak } T_1}{\text{Peak M}}$	Indicator of the relative abundance of proteins to humic-like substances
Total Fluorescence (TF)	TF is calculated integrating the volume under the entire EEM surface, and normalized to the projected excitation-emission area
PARAFAC components	Fluorescence components discriminated by parallel factor analysis. Components are classified according to the position of the excitation and emission peaks and DOM source

Fluorescence spectroscopy and components discrimination by PARAFAC or peak-picking methods has been used for water and wastewater quality monitoring in treatment works. The concentration of the proteinaceous tryptophan-like fluorescent components was found to be sensitive to the biological treatment, and the observed correlations with water quality parameters typically used to evaluate effluents compliance with regulatory standards, such as COD, TOC, BOD5, has suggested the use of this fluorescence component as a tool for water treatment efficacy monitoring in conventional wastewater treatment plants (WWTPs). Recently, correlations between tryptophan-like fluorescence and water quality parameters have been validated in constructed wetland systems as well. The differential spectroscopy approach allowed to find important correlations between various fluorescence components and TOrCs in 10 conventional WWTPs characterized by different secondary treatments (e.g., presence or absence of nitrification and denitrification processes, use of activated sludge unit or rotating biological contactors). Notably, the behavior of (TOrCs) that had very high removals (i.e., triclosan, caffeine and ibuprofen) was correlated with that of the fluorescence indexes associated with aromatic proteins and tyrosine-like components while the behavior of moderately removed atenolol, naproxen, gemfibrozil and trimethoprim was better correlated with the fluorescence index assigned to humic-like substances. A summary of the major aspects of the discussed regression models developed for representative water quality parameters and based on absorbance and fluorescence measurements is presented in Tables below.

Table 5: developed models to predict water quality parameters through absorbance and Fluorescence

Summary of absorbance-based predictive models developed for online monitoring of representative water quality parameters.

Spectroscopic parameter	Target compound	Wastewater treatment/system	Note
$\Delta A_{254}/A_{0,254}$	TrOcs (removal)	Ozonation	Linear regression models; non-applicable for TrCOs with $k_{O3}>10^{-5}$ $M^{-1}s^{-1}$
$\Delta A_{254}/A_{0,254}$	microbial surrogates (deactivation)	Ozonation	Linear regression models
$\Delta A_{254}/A_{0,254}$	TrOcs (removal)	Ozonation	Model based on kinetic approach
$\Delta A_{254}/A_{0,254}$	Degradation products of fluoroquinolone antibiotics (formation)	Ozonation	Non-monotonic correlation models
$\Delta A_{254}/A_{0,254}$ $\Delta A_{280}/A_{0,280}$	Bromate, BDOC (formation)	Ozonation	Non-linear correlation models
$\Delta A_{254}/A_{0,254}$	TrOcs (removal)	Powdered activated carbon (PAC)	Linear and non-linear correlation models
$\Delta A_{254}/A_{0,254}$	TrOcs (removal)	Granular activated carbon (GAC)	Linear regression models
$\Delta A_{254}/A_{0,254}$	TrOcs (removal)	UV/H_2O_2	Linear regression models

Table 4

Summary of fluorescence-based predictive models developed for online monitoring of representative water quality parameters

Spectroscopic parameter	Target compound	Wastewater treatment/system	Note
$\Delta TF/TF_0$	TrOcs (removal)	Ozonation	Linear regression models
$\Delta TF/TF_0$	microbial surrogates (deactivation)	Ozonation	Linear regression models
$\Delta TF/TF_0$	TrOcs (removal)	Ozonation	Model based on kinetic approach
$\Delta TF/TF_0$	Aldehydes and carboxylic acids (formation)	Ozonation	Linear regression models.
$\Delta F/F_0$ (Humic-like fluorescence intensity measured by LED sensor)	Bromate, BDOC (formation)	Ozonation	non-linear correlation models
$\Delta TF/TF_0$	TrOcs (removal)	Powdered activated carbon (PAC)	Linear and non-linear correlation models
$\Delta TF/TF_0$	TrOcs (removal)	Granular activated carbon (GAC)	Linear regression models
$\Delta TF/TF_0$	TrOcs (removal)	UV/H_2O_2	Linear regression models
$\Delta F/F_0$ (tryptophan-like PARAFAC component)	COD, BOD_5, total carbon (removal)	Conventional WWTPs	Linear correlation
$\Delta F/F_0$ (tryptophan-like PARAFAC component)	COD, BOD_5 (removal)	Constructed wetlands	Linear correlation
$\Delta F/F_0$ (peak B)	highly removed TrOCs (e.g., ibuprofen, caffeine, triclosan)	Conventional WWTPs	Linear regression models
$\Delta F/F_0$ (peak C, humic-like PARAFAC components)	Moderately removed TrOCs (e.g., trimethoprim, atenolol, gemfibrozil, naproxen)	Conventional WWTPs	Linear regression models

The most common methods of recording fluorescence spectra for wastewater are excitation-emission matrices (EEM) and synchronous fluorescence spectra (SFS). EEMs represent fluorescence contour maps, which comprise a series of repeated emission scans recorded in a range of excitation wavelengths. SFS are obtained by scanning simultaneously both excitation and emission monochromators at a fixed wavelength interval between them which was 5nm in this study.

4. Material and Methods

4.1 Used water matrix

Water quality parameters of investigated water belongs to Falconara municipal wastewater treatment plant, which is located in Vicinity of Ancona, and is as followed (Table 6):

Table 6: Falconara water matrix

Azoto Ammoniacale	mg/l	0.21 ± 0.17
Azoto Nitrico	mg/l	12.86 ± 3.52
Azoto Nitroso	mg/l	0.03 ± 0.02
Azoto Totale	mg/l	15.49 ± 4
B_O_D_5	mg/l	7.27 ± 3.54
C_O_D	mg/l	38.06 ± 6.13
Cloruri	mg/l	203.38 ± 59.95
Fosforo Totale	mg/l	2.79 ± 0.64
pH	-	7.88 ± 0.13
Solidi Sospesi	mg/l	5.37 ± 3.1
Temperatura	°C	18.57 ± 3

The treated stream is the effluent from the plant and, as expected, is characterized by low COD and TSS (COD is below the 40mg/l and TSS is below 10 mg/l).

4.2 Experimental set-up

The main comparisons regardless of the chemicals added to the sample were undertaken between UV-LED (Figure 9) device and Mercury lamp (Figure 8) respectively with power of 19 W and 80 W.

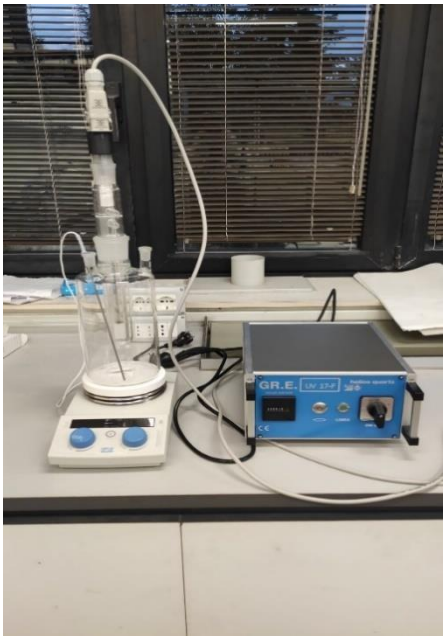

Figure 8: Experimental set-up with mercury lamp

Figure 9: Experimental set-up with LED lamp

The experiment in this study involves the comparison of UV-LED device [ARIA SYSTEM] and a Mercury Lamp with two different Oxidant (H2O2 and Cl2), however before initiating the tests with these two device the process of providing final solution would be to prepare 1500 mL of our effluent water (filtrated) to be mixed thoroughly with two different dosage of hydrogen peroxide [30 , 50 mg/L], and one dosage of Chlorine [5 mg/L] to be exposed with Mercury lamp at time intervals of [130-240-330-460-660-990-1120-1315-1645 seconds] which was calculated based on the UV-Dose assigned to be given through actinometry test. Then the sample relative to each time interval was going through UV-absorbance device of which its scan range was set from 800nm to 200nm that would be covering the majority of constituents withing effluent water while the main wavelength of our interests is 254 nm, which is for the fact that most of constituents composing the organic material in water would fall in the absorption spectra by the mentioned wavelength. After passing all the samples through UV-absorbance the already warmed up Fluorescence device would be checked to make sure the initial setting of the machine corresponds the main purpose of our experiment which are meant to be the excitation range between 220 nm – 450 nm and the emission range of 250 nm – 580 nm plus to check other settings such as device sensitivity to be set on 'Low'. The results of the UV-absorbance device and Fluorescence's would after imported to the Excel for the later elaboration of data to reach to the point where our three main indicators of the Fluorescence [I3 (Ex/Em = 245/440), I4 (Ex/Em = 275/345), I5 (Ex/Em = 345/440)] are obtained. Then the same process was undertaken only this time with UV-LED device carrying 500 mL of sample mixed with the same dosage of hydrogen peroxide as for Mercury lamps only here proportional to the lower aforementioned volume of device inside as the machine capacity was maximum 600 mL, 500 mL would be the optimum volume and given the samples provided within intervals [100-270-330-540-

800-910-1070-1340-1640-1940-2240] would set out again to be analyzed with UV absorption and fluorescence spectrum analysis [Shimadzu RF-6000] however with the same configuration as mentioned earlier.

4.3 Actinometry test

Chemical actinometers are photochemical systems with known quantum yields that can be employed to determine accurate photon fluxes for specific photochemical reactions. A chemical actinometer (also called a dosimeter) is a chemical system (fluid, gas or solid) containing a chromophore C that undergoes a light-induced reaction (at a certain wavelength, λ) for which the quantum yield $\Phi(\lambda)^2$ is known accurately. Measuring the photochemical reaction rate (either –d[C]/dt for the photochemical degradation of C or preferably +d[P]/dt for the photochemical formation of product P formed from the photolysis of C) allows the calculation of the absorbed photon flux qp (abs ,λ) (Einstein s^{-1}). Chemical actinometry, if properly developed, may provide information about dose distribution and therefore could be useful for quantitative prediction of the inactivation of many waterborne microbes, in addition to those used as the challenge organism. Taking into consideration the difficulty in bio-dosimetry to identify a challenged organism that more closely resembles the UV sensitivity of the intended target organisms, the rather complex logistics in performing bio-dosimetry testing, and the high costs associated with off-site bio-dosimetry testing, chemical actinometry is deemed as a promising UV system performance monitoring approach (Stefan.Mihaela I. 2018).

A 0.012 mM uridine solution in 1 mM phosphate buffer was used as the uridine actinometer. An absorbance scan 200– 300 nm was run on all actinometer solutions using UV absorbance device before and after UV exposure. The UV fluence can be directly calculated based on the concentration decrease of uridine actinometer upon exposure to either monochromatic or polychromatic UV sources. For determination of the optimum Time intervals to be corresponding the desired UV Fluence we postulated 9 time intervals each of which with 5 minutes and then the absorbance at each time interval was registered as shown in figures below. After normalizing the data the($\frac{\ln A262^{\circ}}{\ln A262}$)values were elaborated and the plot was drawn to audit the rationale distribution of our data (R) for both UV-LED and MERCURY afterwards to determine the timing proportional to the desired UV Fluence that would meant to be given at each time intervals using the function that later is explained in the Analytical method for the [H'] . Test initially was undertaken by Mercury device and plot of Time Vs degradation was elaborated and afterwards the test was done with UV-LED device at two different Intensity first 50% and since the results of 50% intensity showed more scatter distribution after data normalization the intensity was increased to 75% and then plotted all Versus Time as shown in the two Figures below.

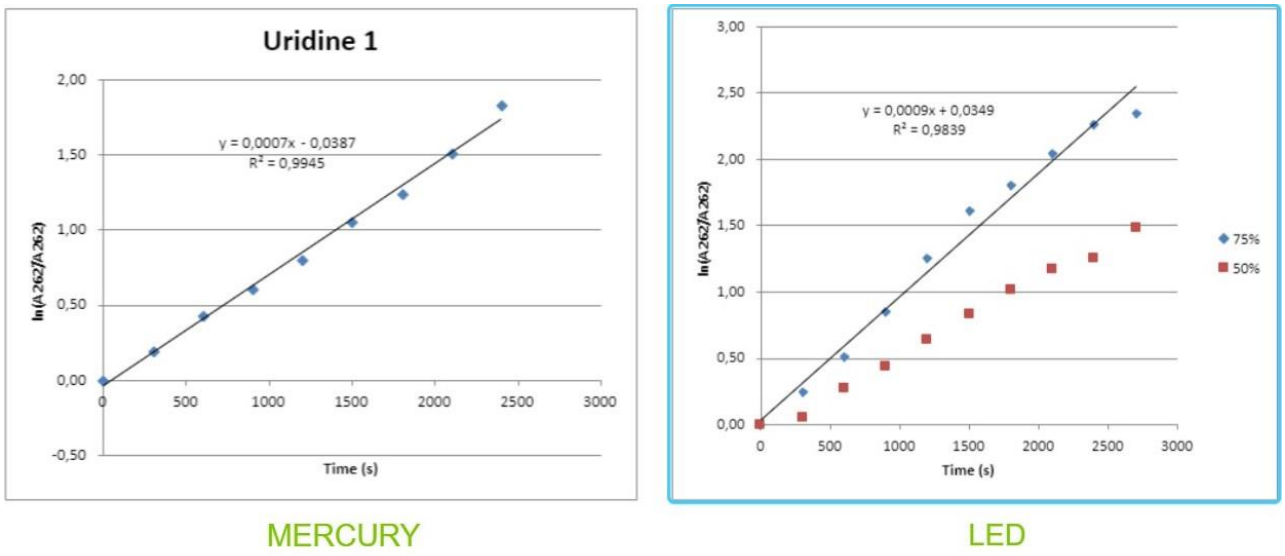

Figure 10: Uridine rate constant for Mercury and LED with 50% and 75% of intensity of irradiation

4.4 Analytical methods

Before going into putting details for how all our results are obtained, it should be said that all the collected sample during experimental tests have been monitored in terms of UV absorbance and Fluorescence with the laboratory equipment shown in Figure 11 and in Figure 12 respectively. In particular, for UV absorbance the SHIMADZU UV-VIS spectrophotometer UV-1900i was used, while for fluorescence measure the Fluorescence Spectrophotometer (SHIMADZU RF-6000) at room temperature (21 ± 1 °C) was used. EEMs were generated by scanning over excitation wavelengths of 220–450 nm at interval of 5 nm and emission wavelengths of 250–580 nm at interval of 1 nm. Excitation and emission slit widths were both set at 5 nm. voltage at 700 V and scanning speed at 1600 nm 1/Min were adopted. Excitation wavelengths below 240 nm and emission wavelengths below 300 nm were removed.

Figure 11: UV-Absorbance 1900i

Figure 12: Fluorescence instrument Shimadzu RF-600

The engineering of an advanced oxidation process consists of the selection of a process to generate Oxidants which mainly here are referred as Hydroxyl Radicals, estimation of the reaction kinetics with the compounds of interest, and design of a reactor in which the reaction will take place. In addition, the presence of background organic and inorganic matter that reacts with the oxidants will reduce the process efficiency for the target compound. Therefore, bench and/or pilot studies are always necessary to determine process efficiency for a given water matrix. According to the study done by [Crittenden et al.2012] hydroxyl Rate constants for few Constituents in water are reported in table below:

Table 7: Hydroxy r_R for few Constituents

Hydroxyl rate constants for selected constituents[a]

Compound name	HO· rate constant, L/mole·s	Compound name	HO· rate constant, L/mole·s
Ammonia	9.00×10^7	Hypobromous acid	2.0×10^9
Arsenic trioxide	1.0×10^9	Hypoiodous acid	5.6×10^4
Bromide ion	1.10×10^{10}	Iodide ion	1.10×10^{10}
Carbon tetrachloride	2.0×10^6	Iodine	1.10×10^{10}
Chlorate ion	1.00×10^6	Iron	3.2×10^8
Chloride ion	4.30×10^9	Methyl tertiary butyl ether (MTBE)	1.6×10^9
Chloroform	5×10^6	Nitrite ion	1.10×10^{10}
CN^-	7.6×10^9	N-Dimethylnitrosamine (NDMA)	4×10^8
CO_3^{2-}	3.9×10^8	Ozone	1.1×10^8
Dibromochloropropane	1.5×10^8	p-Dioxane	2.8×10^9
1,1-Dichloroethane	1.8×10^8	Tetrachloroethylene	2.6×10^9
1,2-Dichloroethane	2.0×10^8	Tetrachloroethylene	1.0×10^7
H_2O_2	2.7×10^7	Tribromomethane	1.8×10^8
HCN	6.0×10^7	Trichloroethylene	4.2×10^9
HCO_3^-	8.5×10^6	Trichloromethane	5.0×10^6
Hydrogen sulfide	1.5×10^{10}	Vinyl chloride	1.2×10^{10}

[a] Adapted from Crittenden et al. (2012).

The second order rate law, $\mathbf{r_R}$, corresponding to the reaction of specific Oxidant, is given by the following expression:

$$r_R = -k_R \cdot C_{H\dot{O}} . C_R$$

$r_R = 5$ second order rate law, $\frac{\text{mole}}{\text{L. s}}$

$k_R =$ second order rate constant for the destruction of R with oxidant radicals, $\frac{\text{L}}{\text{mole. s}}$

$C_{H\dot{O}} \& C_R =$ concentration of Radicals & Constituent , $\frac{\text{mole}}{\text{L}}$

$$t = \left({}^{1}/_{k_R * C_{HO}}\right) * \ln\left(\frac{C_{R_0}}{C_R}\right)$$

Metcalf &eddy

where "t" is the time required to lower the concentration of a Constituent "C_R" for an Oxidant concentration of an ideal plug flow reactor.

Absorption of UV Light:

The absorption of light by a compound in water or other aqueous solution can be described using the Beer-Lambert Law. The absorbance of a solution is a measure of the amount of light absorbed by constituents in the solution using a spectrophotometer at a specified wavelength and over a fixed path length.

$$A(\lambda) = -\log\left(\frac{I}{I_o}\right) = \varepsilon(\lambda) C x = k(\lambda) x$$

Metcalf & eddy

Where:

- "A(λ)" is the absorbance [dimensionless],
- "I" is the light intensity after passing through solution containing constituents of interest at wavelength, [Einstein/cm^{2}s],
- "Io" is the light intensity after passing through a blank solution (i.e., distilled water) of known depth (typically 1.0 cm) at wavelength [Einstein/cm2s]
- "ε_λ" is the base 10 extinction coefficient or molar absorptivity of light absorbing solute at wavelength ʎ [L/mole*cm]
- "ʎ" is the wavelength [nm]
- "C" is the concentration of light absorbing solute [mole/L]
- "X" is the length of light path [cm]
- "K $_ʎ$" is the absorptivity (base 10) [1/cm]

The extinction coefficient is a function of wavelength because as the wavelength decreases more energetic photons are absorbed and the absorptivity of a light absorbing compound increases. Values of the extinction coefficients for several compounds at various wavelengths are given in Table below:

Table 8: General molar absorption and quantum yield of compounds found in Water

Selected quantum yields and extinction coefficients for compounds commonly found in water.

Compound	Primary quantum yield in aqueous phase, mole/einstein	Extinction coefficient at 253.7 nm, L/mole-cm
NO_3^-	–	3.8
HOCl (at 330 nm)	0.23	15
OCl^-	0.23	190
HOCl	–	53.4
OCl^-	0.52	155
O_3	0.5	3300
ClO_2	0.44	108
Sodium chlorite	0.72	–
TCE	0.54	9
PCE	0.29	205
NDMA	0.3	1974
Water	–	0.0000061

Light absorption by a single compound in water was described in the previous analysis. In practice, however, a number of absorbing compounds will be present in solution. The absorption of light as it passes through a solution containing several different compounds may be determined by summing the absorption that would result from each individual compound as shown in the following

expression:

$$\ln\left(\frac{I}{I_o}\right) = -\left[\sum \varepsilon'(\lambda)_i C_i\right] x$$

Metcalf & Eddy

Where:

- "$\varepsilon'(\lambda)_i = 2.303\varepsilon(\lambda)_i$" is the extinction coefficient of compound i at wavelength l (base e), [L/(mole*cm)];
- "C_i" is the concentration of compound i, [mole/L]

Energy Input for Photolysis:

$$P_R = \frac{P\eta}{N_P V h\nu}$$

P_R = photonic energy input per unit volume of the reactor, einstein/L·s
P = lamp power, J/s (W)
h = Planck's constant, 6.62×10^{-34} J·s
η = output efficiency at the wavelength of interest (as a fraction)
N_P = number photons per mole (as einstein), 6.023×10^{23} 1/einstien
V = reactor volume, L
$\nu = \frac{c}{\lambda}$ = frequency of light, 1/s
c = the speed of light, 3.00×10^8 m/s
λ = wavelength of the light, m

The lamp output and reactor size can be used to estimate the energy input for the photolysis reaction. The theoretical maximum photonic energy input per unit volume of the reactor can be determined using the function expressed. While the expressed analysis is satisfactory for a theoretical assessment, the actual performance of a photoreactor is expected to be lower than computed using equation above due to light being absorbed by the reactor walls or blocked by the precipitate that forms on the lamp sleeve. While a safety factor specific to a particular system could be applied to compensate for these inefficiencies, pilot studies are used to obtain more reliable design criteria.

Rate of Photolysis:

The rate at which a compound is photolyzed depends on the rate and frequency of photon absorption. The volumetric photon absorption rate derived from:

$$\boldsymbol{I_v = -\frac{dI}{dx} = \varepsilon'(\lambda) \cdot c \cdot I_0 \cdot e^{\varepsilon'(\lambda).C.x}}$$

Metcalf & eddy

where:

- "$\boldsymbol{I_v}$" is the rate that photons are absorbed per volume of solution at a particular point, [Einstein/cm^3*s]
- "$\varepsilon'(\lambda)_i = 2.303\varepsilon(\lambda)_i$" is the extinction coefficient of compound *i* at wavelength l (base e), [L/(mole.cm)]

The quantum yield:

The quantum yield is a quantity used to describe the frequency at which photon absorption results in a photolysis reaction and is specific to the type of compound and the wavelength. The quantum yield, Φ_λ, is defined as being equal to the number of photolysis reactions divided by the number of photons absorbed by the molecule as follows:

$$\Phi_\lambda = -\frac{r_R}{\boldsymbol{I_v}} = \frac{REACTION\ RATE}{RATE\ OF\ PHOTON\ ABSORPTION}$$

Metcalf & eddy

Φ_λ = quantum yield at wavelength $\boldsymbol{\lambda}$, $\left(\frac{\text{mole}}{\text{einstein}}\right)$

r_R = photolysis rate, $\left(\frac{\text{mol}}{cm^3.s}\right)$

Typically, the light absorption by the component that is targeted for removal is minor as compared to the light absorption by the background water matrix (Crittenden et al., 2012). The pseudo first order rate law for the photolysis reaction is:

$$r_{Avg} = \left[\Phi_\lambda . \mathrm{P_R} . \frac{\boldsymbol{\varepsilon'(\lambda)}}{\boldsymbol{k'(\lambda)}}\right] . C = k . C$$

Metcalf & eddy

r_{avg}	= overall average photolysis rate of the constituent in the reactor, mole/L·s
$\phi(\lambda)$	= quantum yield of the constituent at wavelength λ, mole/einstein
$\varepsilon'(\lambda)$	= the extinction coefficient of the constituent (base *e*), L/mole·cm
C_i	= the concentration of the constituent, mole/L
$k'(\lambda)$	= measured absorptivity of the water matrix at wavelength (base *e*) λ, 1/cm
k	= pseudo-first order rate coefficient, 1/s

UV exposures were conducted under bench scale collimated beam type (both with LED and Mercury device respectively with the peak irradiation of 272 nm and 252 nm). 10 mL of the uridine actinometer solution, were irradiated independently. Subtilis systems were in determining the exposure times for the MP system, radiometer readings were first corrected by the Petri factor, depth, and water absorbance for each wavelength. Exposure times were then calculated by dividing targeted fluence by the corrected radiometer fluence rate irradiance readings. To determine P-UV exposure time, a fluence per pulse value, which was treated as a fluence rate equivalent for P-UV, was first determined

by setting the radiometer into an integrating mode to collect data over a period of pulses. This value was also corrected by the Petri factor and water absorbance factors. Exposure times were then determined by the following calculation:

$$\text{Exposure time} = \frac{\text{targeted fluence}}{\text{UV fluence per pulse}}$$

A 0.012 mM uridine solution in 1 mM phosphate buffer was used as the uridine actinometer. An absorbance scan 200– 300 nm was run on all actinometer solutions using UV-1900i spectrophotometer before and after UV exposure. The UV fluence can be directly calculated based on the concentration decrease of uridine actinometer upon exposure to either monochromatic or polychromatic UV sources.

$$H' = \frac{\ln A262^{\circ}}{\ln A262.(2.303).1{,}000.\varepsilon_{\lambda}\cdot\phi\cdot t} * U * \ t$$

where "H′" represents the directly calculated UV fluence [mJcm^{-2}]; "A262°" and "A262" [unitless] represent the absorbance at 262 nm before and after irradiation, respectively; "$(\frac{\ln A262^{\circ}}{\ln A262})/t$" is the slope of the linear regression versus exposure time t(s) and M^{-1}.cm^{-1}=molar absorption coefficient of uridine for the irradiation wavelength e.g., 254 nm. It should be noted that when calculating the fluence from a polychromatic light source, the molar absorption coefficient for the peak absorption wavelength 262 nm should be used. The ε_{262}value used in this study is 10, 185 M^{-1} cm^{-1}, which was determined experimentally. The value of 10, 140 M^{-1} cm^{-1}was reported in a previous study for the same chemical. In this study, the initial peak absorbance of actinometer in the reactor vessel is 272 nm for the test done with LED device and 252nm for when the test was done with mercury device and continuously decreases upon UV exposure, which ensures less than 6% of error from the calculation method. In order to obtain some insights in the directly calculated fluence value, the derivation of Eq above is outlined next. It has been reported that uridine undergoes first order degradation upon UV irradiation .Based on first order kinetics and the light absorption theory, when absorbance of the actinometer solution is very small, at wavelength ʎ the rate constant of the uridine decay

$K_{ʎ}$ (s^{-1}) is expressed as:

$$K_{ʎ} = 2.303 * 1{,}000 * \left(\frac{E'_{\lambda_0}}{U_{\lambda}}\right)\cdot\varepsilon_{\lambda}\cdot\Phi_{\lambda}$$

where E'_{λ_0} =incident fluence rate (mW $^{cm-2}$)emitted at wavelength ʎ (exclusive of the portion reflected by solution surface)ε_{λ}=molar absorption coefficient (M^{-1} cm^{-1}) of uridine at wavelength ʎ;Φ_{λ}=

quantum yield at ʎ (mole einstein^{-1}); U_λ= photon energy at emission wavelength ʎ (milli Joule einstein^{-1}).

Expanding the equation for

$K_ʎ$: total→ $K = \sum K \rightarrow \sum \left\{2.303 \times \left(\frac{E'_{\lambda 0}}{U_\lambda}\right) \times \varepsilon_\lambda \times \phi_\lambda\right\}$

$\varepsilon_\lambda = x_\lambda \cdot \varepsilon_{262}$

$$\frac{ln(C_0 \,/\, C_t)}{t} = 2.303 * \varepsilon_{262} \times \phi * \{\sum \left[x_\lambda * \left(\frac{E'_{\lambda 0}}{U_\lambda}\right)\right]\} H' = \Sigma \left[\left(\frac{E'_{\lambda_0}}{U_\lambda}\right) * x_\lambda\right] * t * U$$

In the Figure 13 the general algorithm for carrying out the actinometry test is introduced.

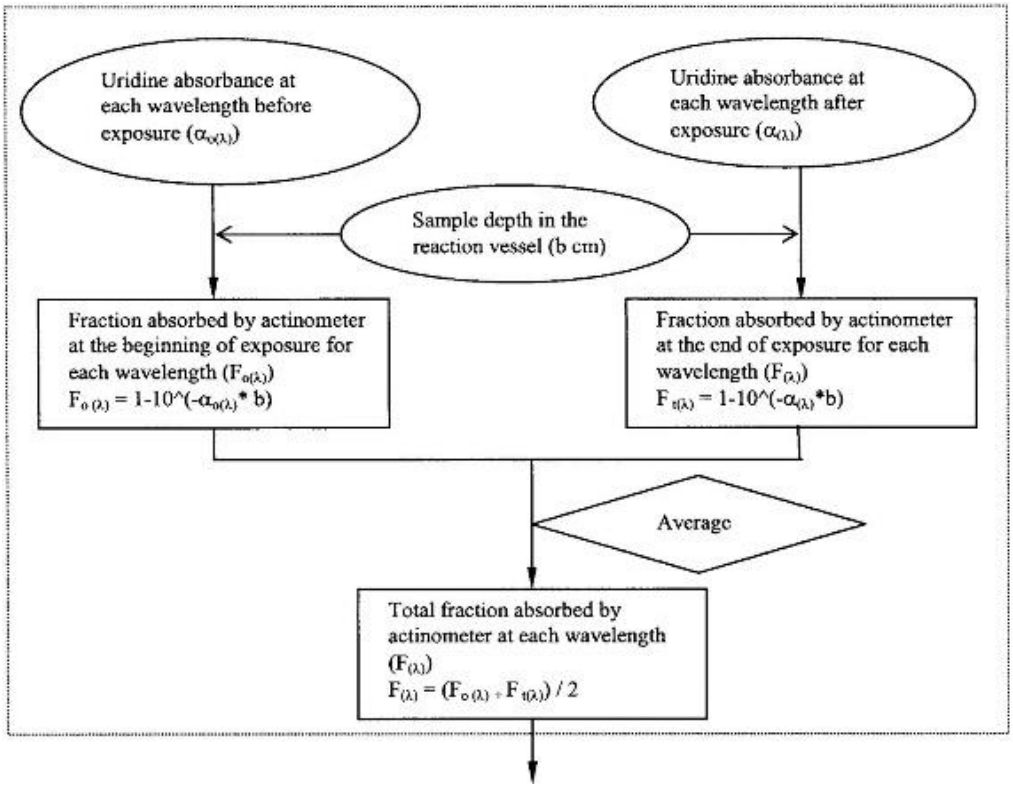

Figure 13: General algorithm of Actinometry test with Uridine.

Electrical energy consumption:

For calculating the electrical energy there are two main aspects that we would consider during this test, the first one was the electrical energy for UV irradiation ($E_{EO,UV}$) and the second one the equivalent electrical energy for the radical promoter consumption ($E_{EO,RP}$):

$E_{EO} = E_{EO,UV} + E_{EO,[RP]}$.

(Sgroi et al, 2021)

The energy consumption of the UV lamp was calculated by plotting the kWh of each UV-DOSE (obtained knowing the electrical consumption of the two experimental equipment used) versus the

degradation rate and interpolating the measured point to have a function applicable for each degradation rate. In our case we considered 50% and 90% degradation. The second contribution was calculated considering the following energy consumption per mole of utilized radical promoter: $E_{EQ,chlorine}$ = 0.851 kWh M^{-1} and $E_{EQ,H2O2}$ = 0.241 kWh M−1 (Sgroi et al, 2021).

In the following table, the calculation of the equivalent electrical energy for the radical promoter consumption in our specific case are reported:

Table 9: Electrical energy for the radical promoter consumption

		H2O2 30 mg/l	**H2O2 50 mg/l**	**Cl2 5 mg/l**
Specific energy consumption	kWh M^{-1}	0.241	0.241	0.851
M of the dosage	M	0.00088	0.0015	0.00071
Energy consumption	kWh	0.00021	0.00035	0.00060

5. Results and discussion

In this section the detailed analysis of all the different tests done with both UV experimental set-up will be discussed. Results reported initially for H2O2 and then for Cl2, and finally a comparison between the two oxidants will be carried on. Afterwards provided all desired data we would arrive at a point where results about energy calculation would be reported and discussed.

5.1 Results with H2O2

At first test with H2O2 were done, two test with 30-50 mg/l results will be discussed first for the test with 30 and then with 50 for both mercury and led experimental equipment. The main desired outcome of our test are of those plots showing the comparison of rate of constants of decomposition due to H2O2 addition withing different dosage plus the UV absorbance at 254 nm degradation and the degradation at three main Fluorescence indicators as explained earlier. At first results with the mercury lamp will be shown, and then the results with LED lamp and the final comparison.

5.1.1 Results with Mercury lamp

Test with Mercury lamp included both dosage of H2O2, in Table 10 data extrapolated from UV and Fluorescence laboratory equipment are reported, for the test with 30 mgH2O2/l.

Table 10: Initial data, Mercury 30 mg/L H2O2

			Fluorescenze		
Time (s)	**Dose (mJ/cm2)**	**Abs (254 nm)**	**I3**	**I4**	**I5**
0	0	0.1350	0.67	0.38	0.74
130	100	0.1270	0.62	0.42	0.65
240	184	0.1190	0.26	0.10	0.31
330	250	0.1180	0.65	0.30	0.65
460	350	0.1120	0.46	0.21	0.50
660	500	0.1020	0.36	0.14	0.42
990	750	0.0920	0.26	0.07	0.31
1120	850	0.0950	0.26	0.08	0.30
1315	1000	0.0860	0.17	0.05	0.25
1645	1250	0.0760	0.12	0.008	0.19

Data obtained from the instrument were at first represented in graphic form as reported in Figure 14. From the figure it can be noticed that UV (254 nm) is less sensible than the fluorescence indices which show a higher reduction during the test.

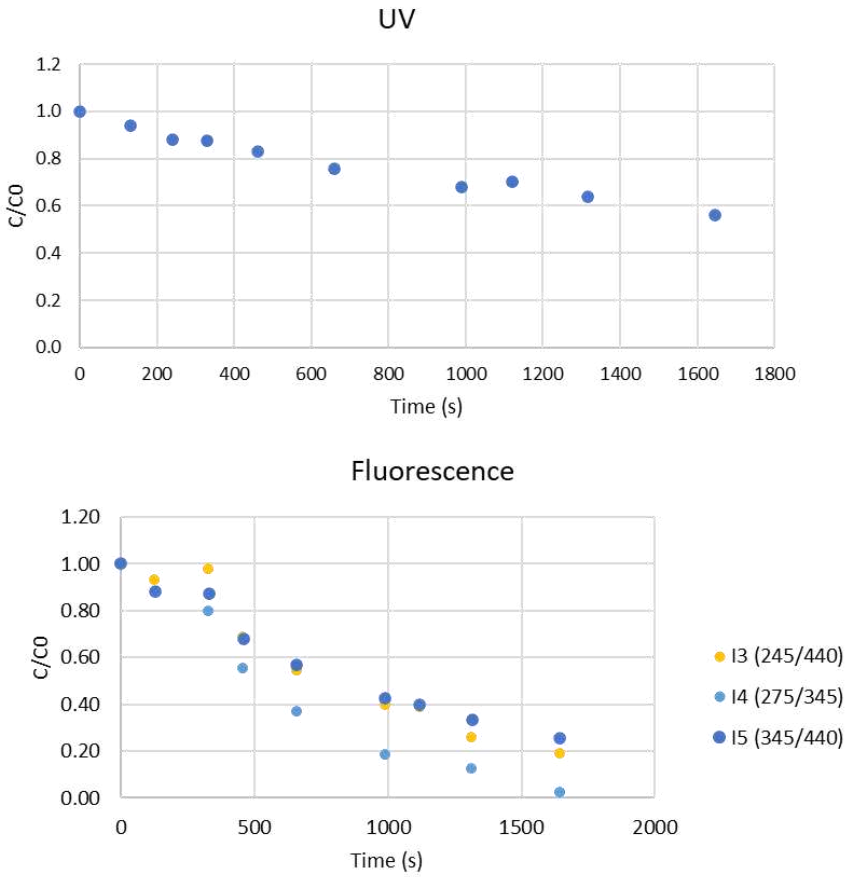

Figure 14: UV (254 nm) and Fluorescence (I3-I4-I5) C/C0 trend in time with Mercury lamp and 30 mgH2O2/l

All data have been linearized (Figure 15) to subsequently reach us on measure of the degradation rate (kobs) of both UV (254 nm) and the three fluorescence indices (Figure 16). For this test, higher degradation trend was observed with I4 fluorescence indicator.

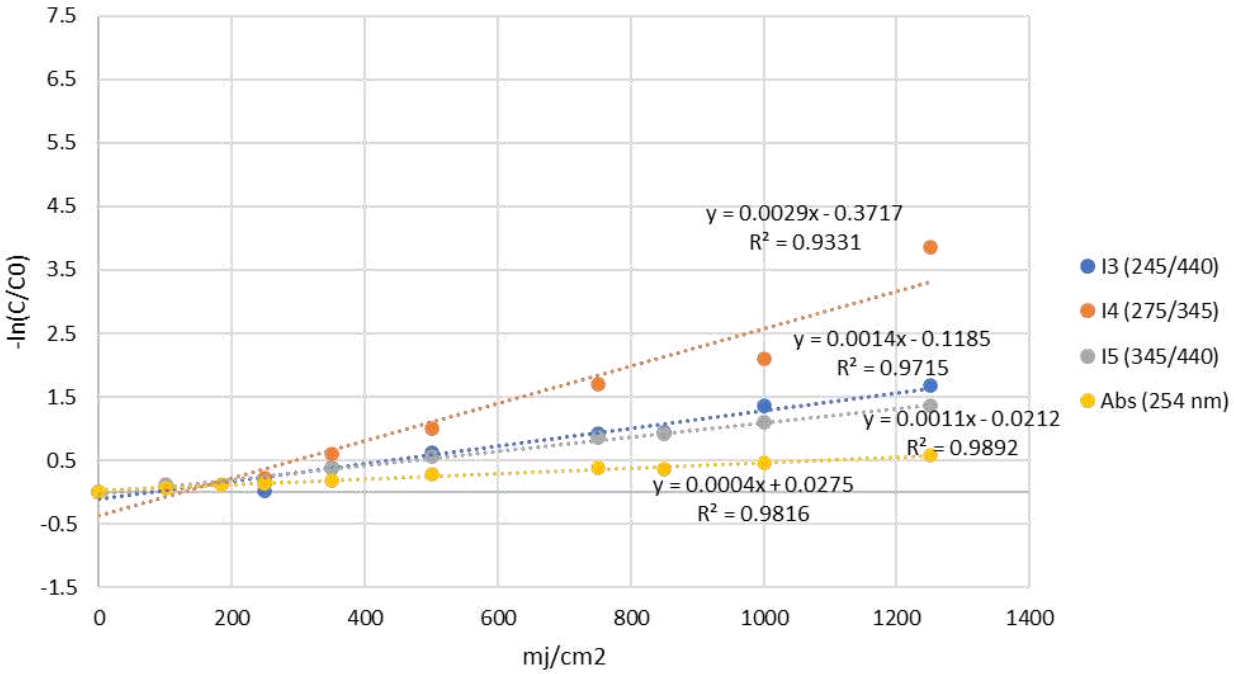

Figure 15: Linearization (test with Mercury lamp and 30 mgH2O2/l)

Mercury + 30mg/l H2O2	kobs	R2
Abs	0.0004	0.9816
I3	0.0014	0.9715
I4	0.0029	0.9331
I5	0.0011	0.9282

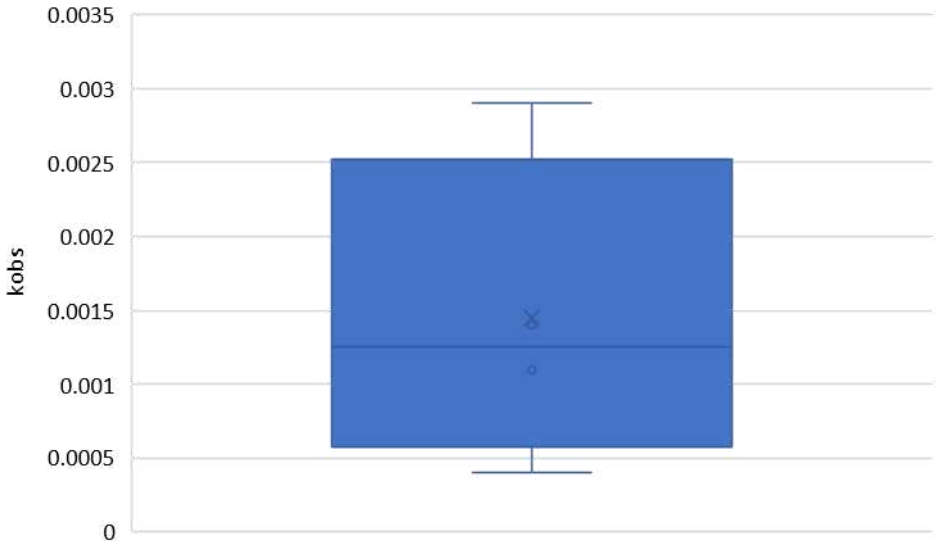

Figure 16: Kobs and box-plot representation (test with Mercury and 30 mgH2O2/l)

Same results are reported also with the test performed with 50 mgH2O2/l. In Table 11 data extrapolated from the laboratory equipment are reported, while in Figure 17 the (C/C0) trend is represented. Also in this case fluorescence indices showed higher removal than UV (254 nm).

Table 11: Initial data, Mercury 50 mg/L H2O2

			Fluorescenze		
Time (s)	**Dose (mJ/cm2)**	**Abs (254 nm)**	**I3**	**I4**	**I5**
0	0	0.1560	0.78	0.55	0.76
130	100	0.0980	0.35	0.22	0.43
240	184	0.1060	0.26	0.10	0.31
330	250	0.1010	0.26	0.10	0.31
460	350	0.0800	0.09	0.01	0.16
660	500	0.0760	0.06	0.01	0.13
990	750	0.0600	0.02	0.00	0.08
1120	850	0.0630	0.04	0.01	0.10
1315	1000	0.0450	0.015	0.006	0.08
1645	1250	0.0500	0	0	0.04

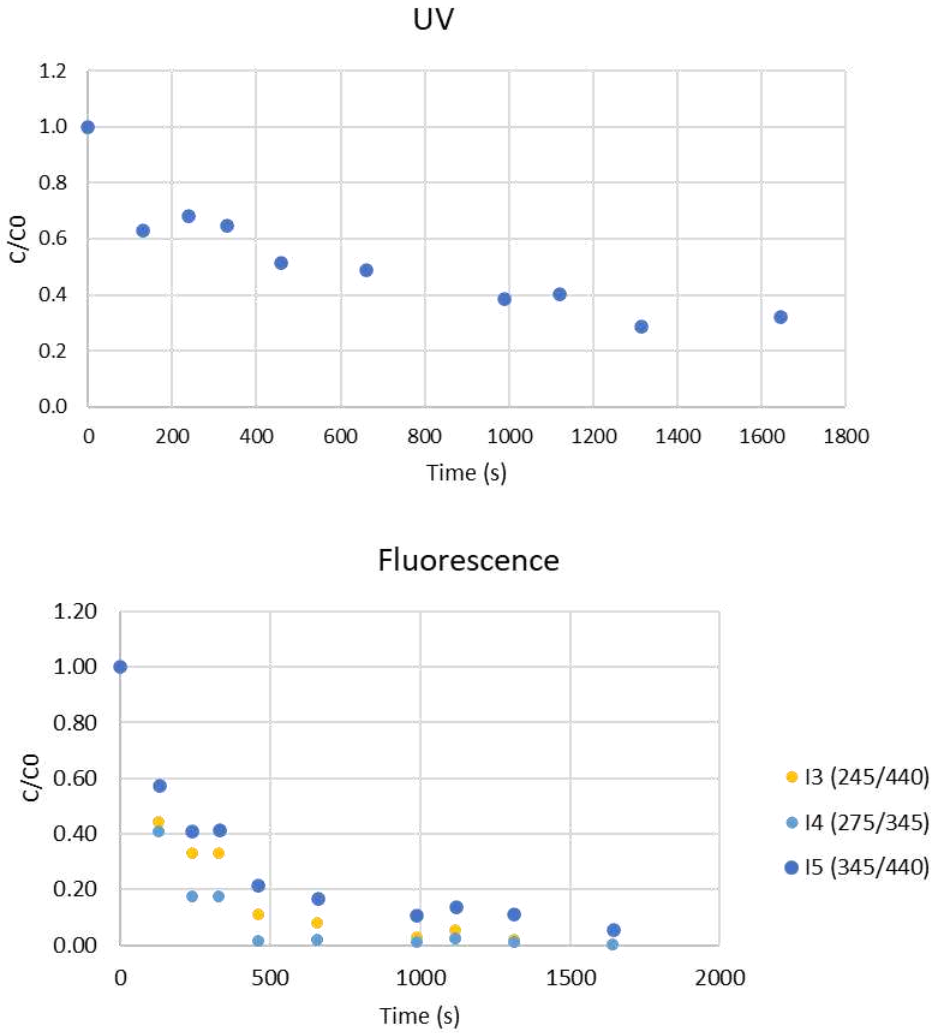

Figure 17: UV (254 nm) and Fluorescence (I3-I4-I5) C/C0 trend in time with Mercury lamp and 50 mgH2O2/l

Finally results about linearization and degradation rate are reported in the following Figure 18 and Figure 19. Also in this case fluorescence indicator I4 showed the best performances with constant

rate (Kobs) of 0.0043. while, at the same time, I4 is also the parameter showing the worst interpolation with R2 equal to 0.73.

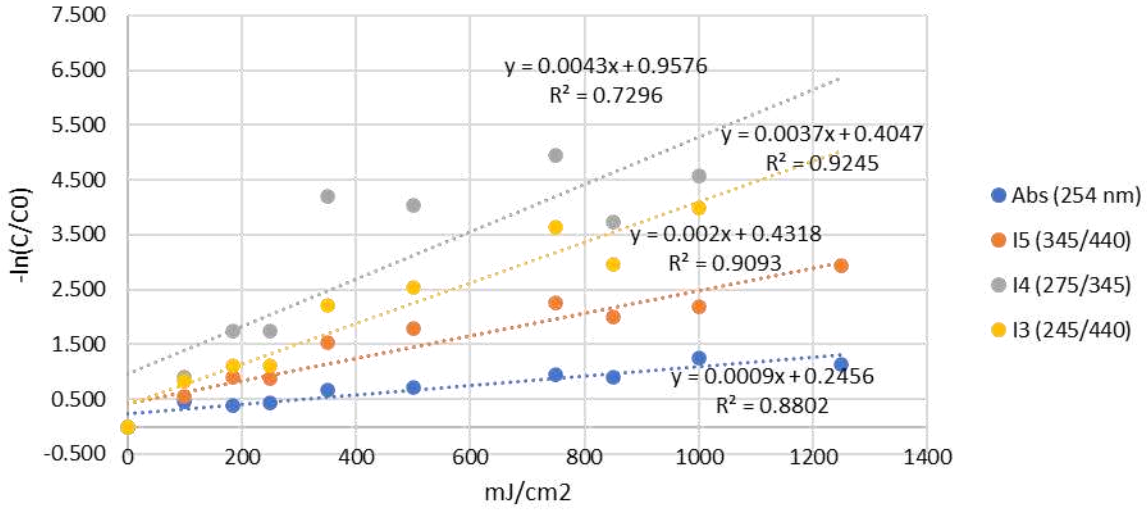

Figure 18: Linearization (test with Mercury lamp and 50 mgH2O2/l)

Mercury + 50mg/l H2O2	kobs	R2
Abs	0.0009	0.8802
I3	0.0037	0.9245
I4	0.0043	0.7296
I5	0.002	0.9093

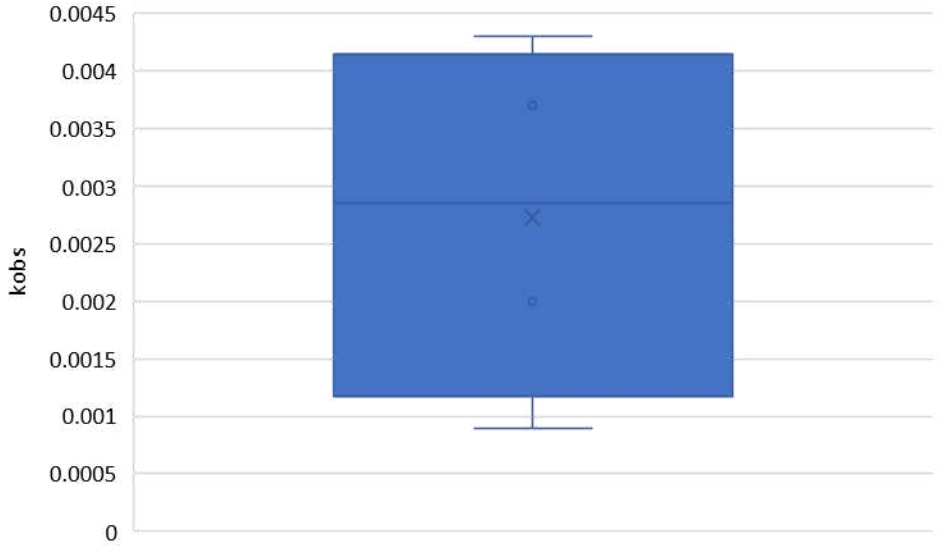

Figure 19: Kobs and box-plot representation (test with Mercury and 50 mgH2O2/l)

Comparing the results with the two concentration of H2O2 with Mercury UV lamp, it is possible to notice, as expected an increasing in the performances with a higher H2O2 dosage (Figure 20). Kobs increased both for UV (254 nm) and for the three fluorescence indices.

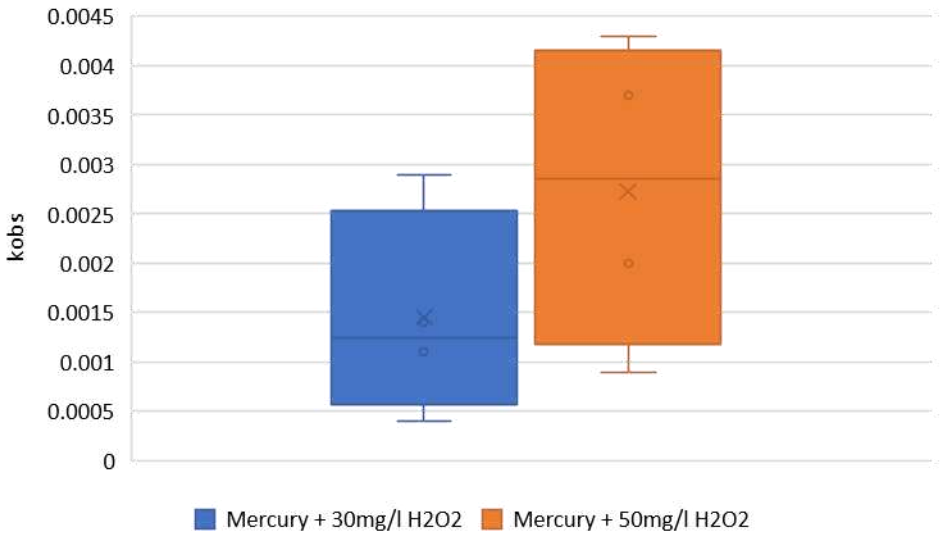

Figure 20: Comparison between 30 mgH2O2/l and 50 mgH2O2/l with Mercury lamp

5.1.2 Results with UV-LED lamp

Both tests and elaboration have been done also with the UV-LED lamp. Considering the dosage of 30 mgH2O2/l, Table 12 shows data extrapolated from UV and Fluorescence laboratory equipment.

Table 12: Initial data, LED 30 mg/L H2O2

			Fluorescenze		
Tempo (s)	**Dose (mJ/cm2)**	**Abs (254 nm)**	**I3**	**I4**	**I5**
0	0	0.1420	0.7411	0.5999	0.7687
100	100	0.1320	0.6590	0.5233	0.6556
270	250	0.1380	0.6163	0.4198	0.6834
380	350	0.1310	0.6384	0.3767	0.7021
540	500	0.1310	0.5960	0.3347	0.6389
800	750	0.1270	0.2564	0.5780	0.5220
910	850	0.1180	0.5099	0.2001	0.5640
1070	1000	0.1130	0.5342	0.2314	0.5300
1340	1250	0.1090	0.4818	0.2617	0.4644
1640	1647	0.1010	0.3383	0.1281	0.4295
1940	1936	0.0950	0.3502	0.1215	0.3699
2240	2246	0.0900	0.2696	0.0518	0.3335

Graphical representation of data is reported in Figure 21, showing again that fluorescence has higher sensibility than UV (254 nm). Linearization and Kobs are reported in Figure 22 and Figure 23. I4 is the parameter degradation rate.

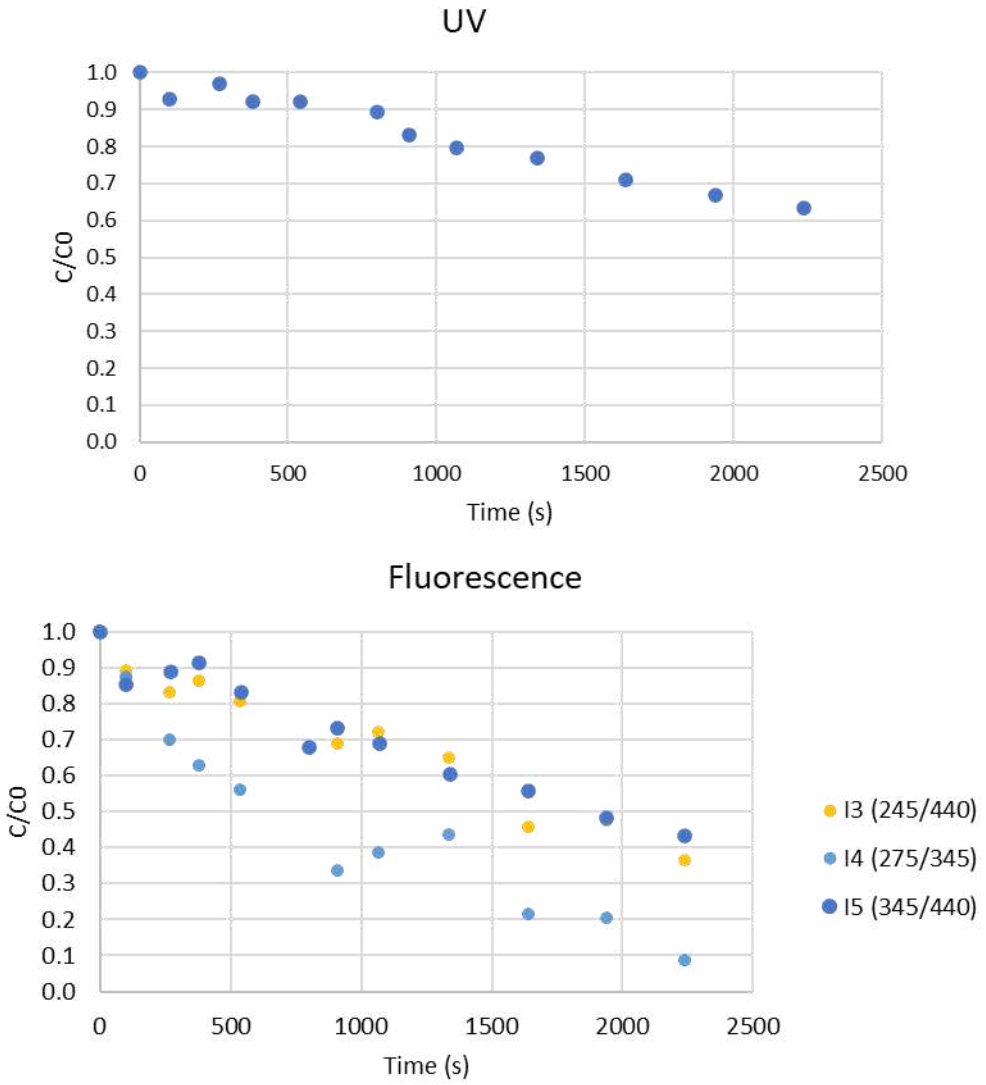

Figure 21: UV (254 nm) and Fluorescence (I3-I4-I5) C/C0 trend in time with UV-LED lamp and 30 mgH2O2/l

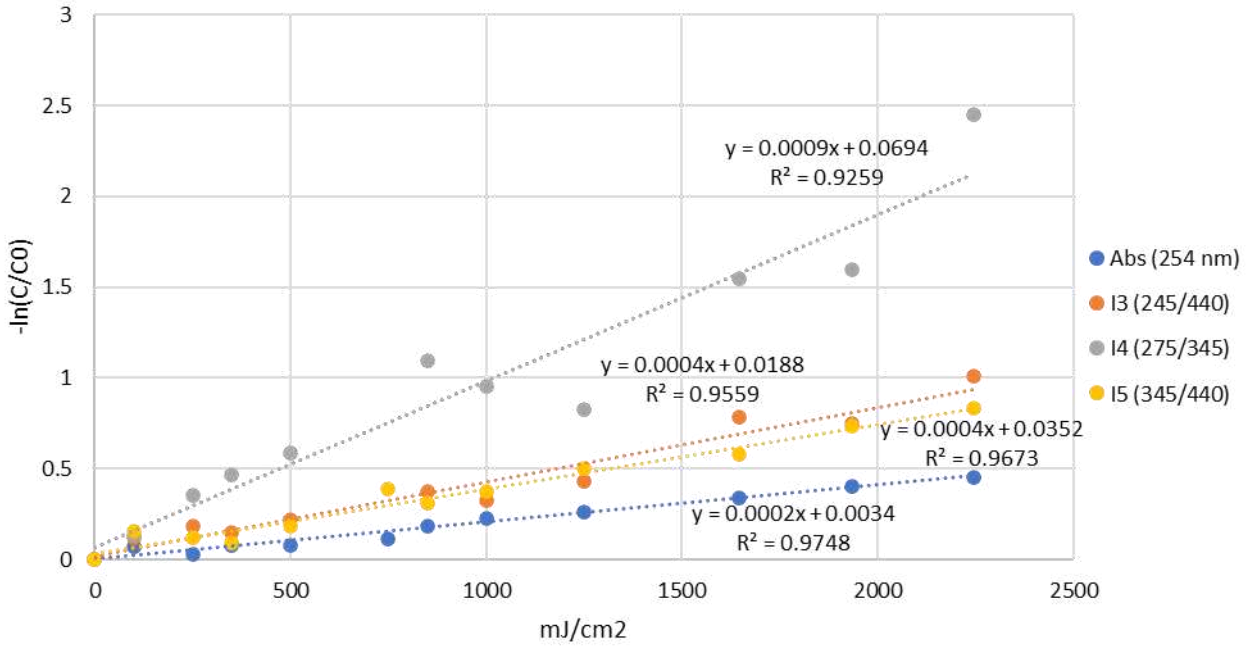

Figure 22: Linearization (test with UV-LED lamp and 30 mgH2O2/l)

LED + 30mg/l H2O2	kobs	R2
Abs	0.0002	0.9748
I3	0.0004	0.9559
I4	0.0009	9259
I5	0.0004	0.9673

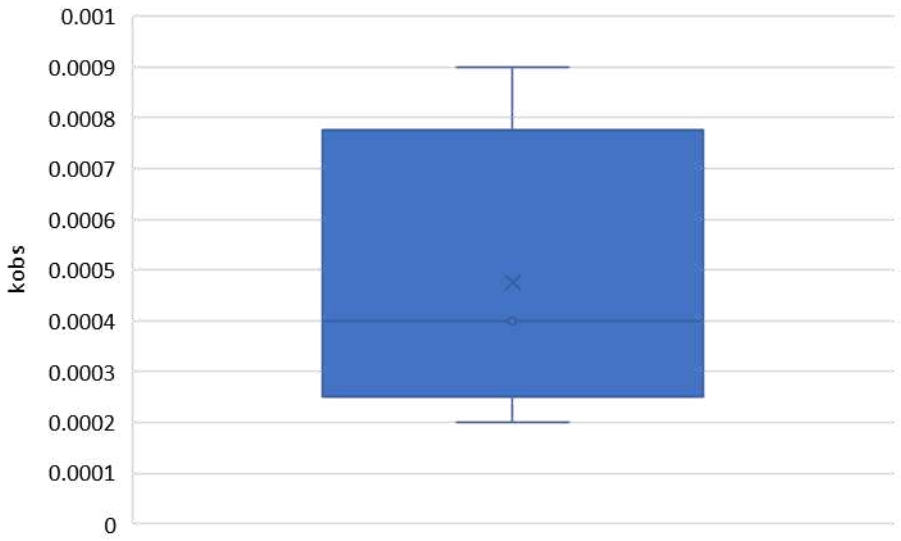

Figure 23: Kobs and box-plot representation (test with UV-LED and 30 mgH2O2/l)

Same results are reported also with the test performed with 50 mgH2O2/l. In Table 13 data extrapolated from the laboratory equipment are reported, while in Figure 24 the (C/C0) trend is represented.

Table 13: Initial data, UV-LED 50 mg/L H2O2

			Fluorescenze		
Time (s)	**Dose (mJ/cm2)**	**Abs (254 nm)**	**I3**	**I4**	**I5**
0	0	0.1510	0.7973	0.5454	0.7698
100	100	0.1460	0.6600	0.5059	0.6674
270	250	0.1440	0.8412	0.6364	0.8838
380	350	0.1390	0.6189	0.3628	0.6076
540	500	0.1330	0.6272	0.3295	0.6064
800	750	0.1290	0.5258	0.2436	0.5220
910	850	0.1290	0.4975	0.1961	0.5038
1070	1000	0.1270	0.4006	0.2655	0.4736
1340	1250	0.1180	0.3132	0.1148	0.3895
1640	1647	0.1130	0.2683	0.0717	0.3408
1940	1936	0.1030	0.2576	0.0487	0.2889
2240	2246	0.1030	0.2098	0.0739	0.2675

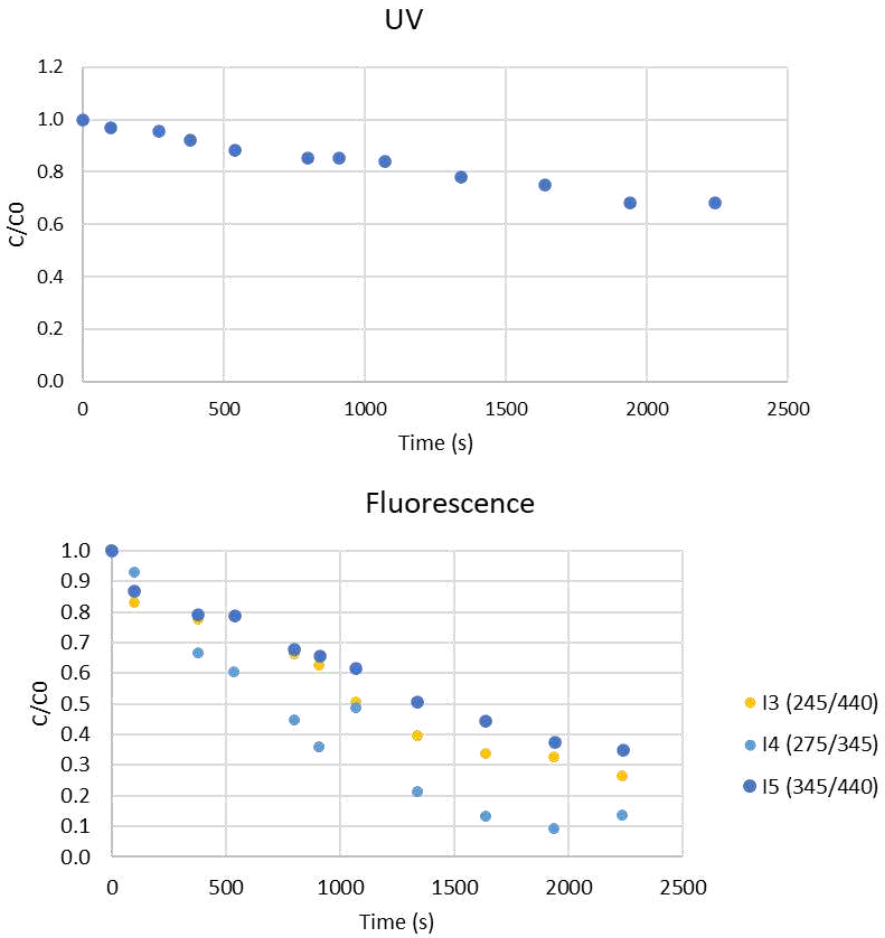

Figure 24: UV (254 nm) and Fluorescence (I3-I4-I5) C/C0 trend in time with UV-LED lamp and 50 mgH2O2/l

Finally results about linearization and degradation rate are reported in the following Figure 25 and Figure 26. Also in this case fluorescence indicator I4 showed the best performances with Kobs of 0.0011.

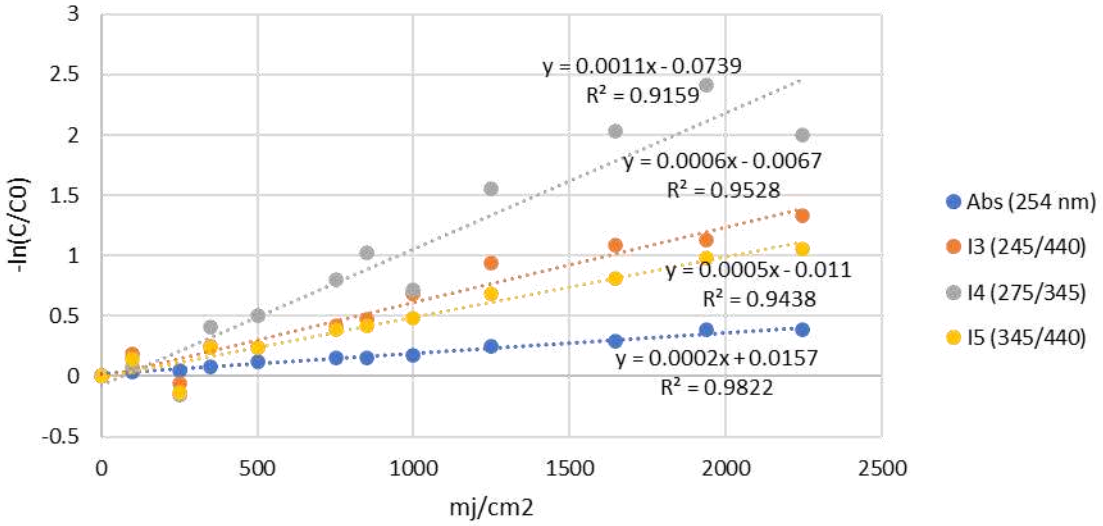

Figure 25: Linearization (test with UV-LED lamp and 50 mgH2O2/l)

LED + 50mg/l H2O2	kobs	R2
Abs	0.0002	0.9822
I3	0.0006	0.9528
I4	0.0011	0.9159
I5	0.0005	0.9438

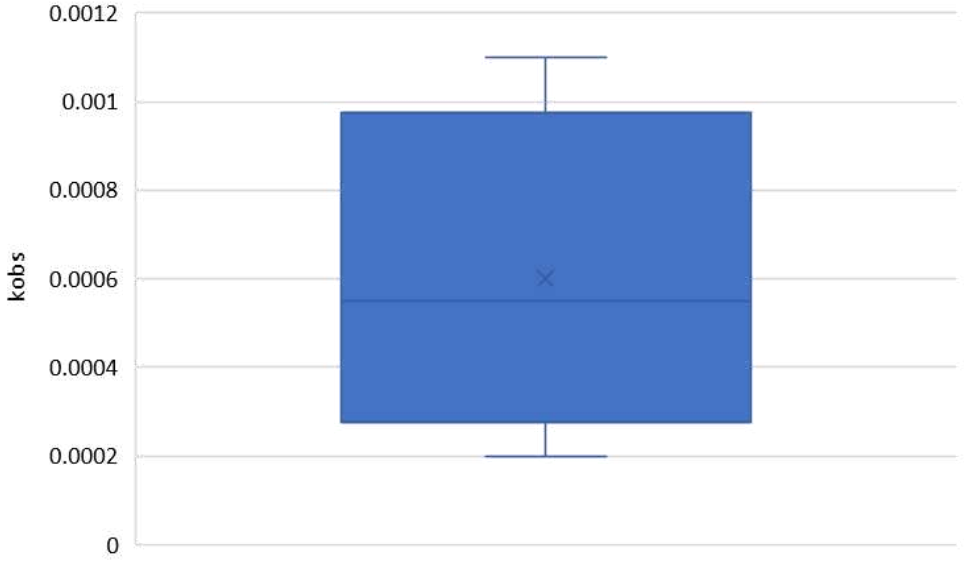

Figure 26: Kobs and box-plot representation (test with UV-LED and 50 mgH2O2/l)

Comparing the results with the two different concentrations relative to H2O2 with UV-LED lamp, it is observed that better performances with higher dosage of H2O2 took place (Figure 27).

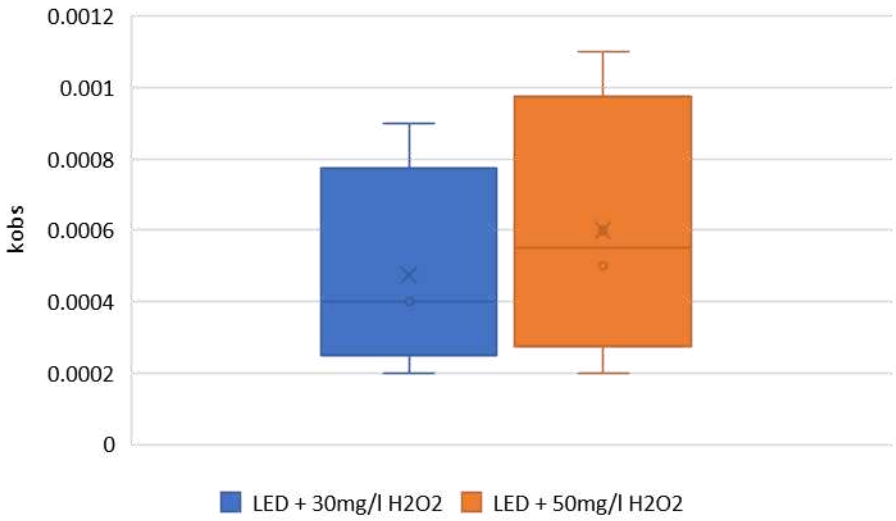

Figure 27: Comparison between 30 mgH2O2/l and 50 mgH2O2/l with UV-LED lamp

5.1.3 Comparison between Mercury and LED UV lamps

Finally, in Figure 28 the result of comparison between two UV lamps is represented. In general, it is possible to see that Mercury lamp demonstrate better performances than LED with (Kobs) increasing from 0.0002-0.0011 while for the UV-LED to 0.0004-0.0043 for Mercury lamp.

Figure 28: comparison between Mercury and UV-LED lamp with H2O2 as oxidant

5.2 Results with Cl2

Same procedure has been done also using Cl2 as oxidant. In this case only the concentration of 5 mgCl2/l have been tested comparing the results obtained with UV-LED and UV-Mercury lamp.

Considering mercury lamp first, in Table 14 data extrapolated from laboratory instruments are reported, and the graphical representation is reported in Figure 29.

Table 14: Initial data, Mercury lamp 5mg/L Cl2

			Fluorescenze		
Time (s)	**Dose (mJ/cm2)**	**Abs (254 nm)**	**I3**	**I4**	**I5**
0	0	0.153	0.113	0.139	0.045
100	100	0.135	0.058	0.072	0.037
270	250	0.123	0.034	0.081	0.035
380	350	0.115	0.023	0.025	0.031
540	500	0.112	0.011	0.039	0.027
800	750	0.100	0.006	0.025	0.023
910	850	0.088	0.000	0.014	0.020
1070	1000	0.085	0.000	0.009	0.018
1340	1250	0.084	0.001	0.018	0.022
1640	1647	0.070	0.000	0.000	0.010
1940	1936	0.061	0.000	0.000	0.005
2240	2246	0.060	0.000	0.000	0.010

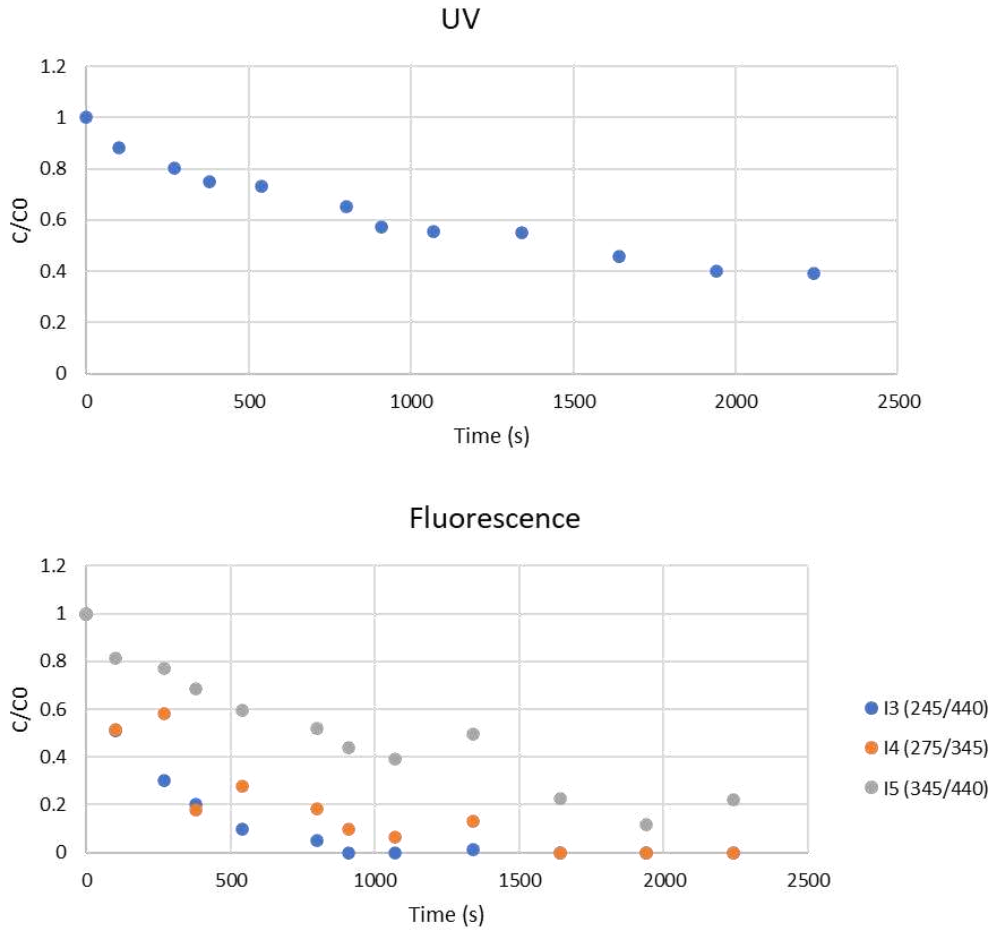

Figure 29: UV (254 nm) and Fluorescence (I3-I4-I5) C/C0 trend in time with Mercury lamp and 5 mgCl2/l

Linearization was done for the aim of measuring the degradation rate; subsequent results are demonstrated in the following Figure 30 and Figure 31. As the figures illustrate higher degradation

rate were related to I3 fluorescence index (kobs = 0.0034), while lower with UV absorbances at 254 nm (kobs = 0.0004).

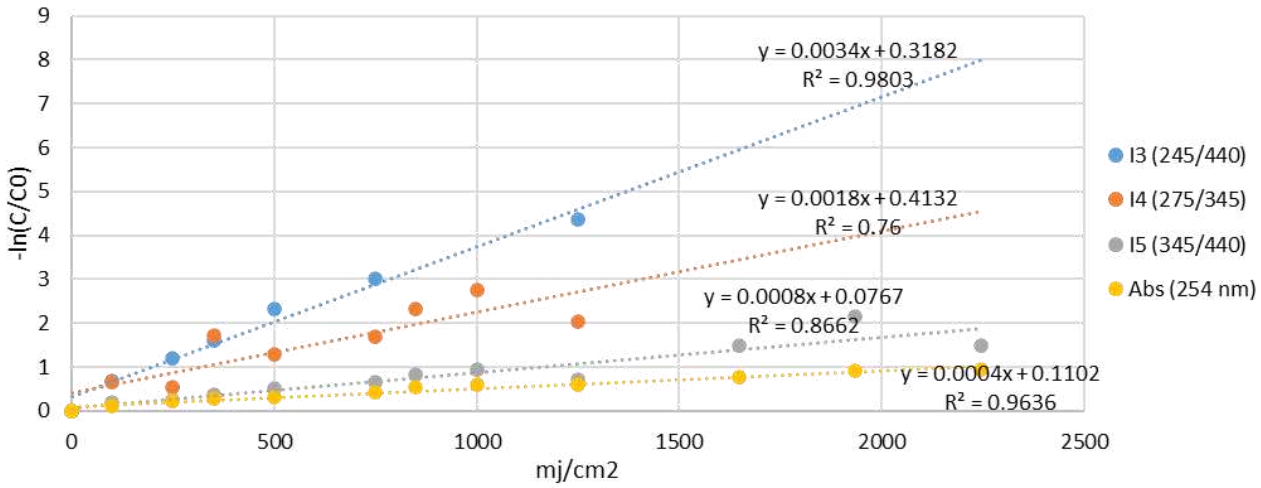

Figure 30: Linearization (test with Mercury lamp and 5 mgCl2/l)

Mercury + 5mg/l Cl2	kobs	R2
Abs	0.0004	0.9636
I3	0.0034	0.9803
I4	0.0018	0.76
I5	0.0008	0.8662

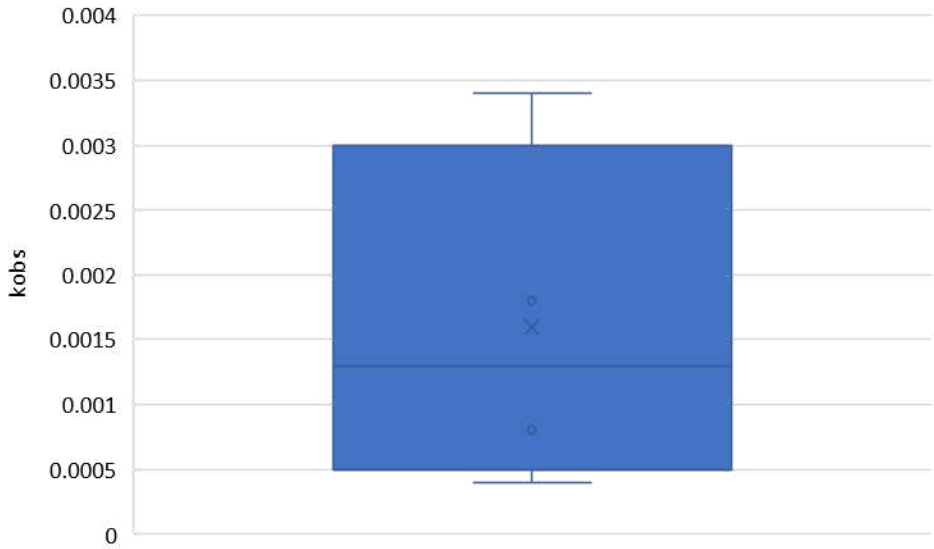

Figure 31: Kobs and box-plot representation (test with Mercury lamp and 5 mgCl2/l)

Same elaboration has been done also for the UV-LED lamp. In Table 15 and in Figure 32 initial data are reported.

Table 15: Initial data, UV-LED lamp 5mg/L Cl2

			Fluorescenze		
Time (s)	**Dose (mJ/cm2)**	**Abs (254 nm)**	**I3**	**I4**	**I5**
0	0	0.143	0.106	0.157	0.064
100	100	0.143	0.135	0.211	0.091
270	250	0.132	0.085	0.094	0.059
380	350	0.117	0.040	0.051	0.045
540	500	0.101	0.017	0.028	0.034
800	750	0.089	0.009	0.018	0.031
910	850	0.082	0.004	0.009	0.029
1070	1000	0.075	0.001	0.001	0.023
1340	1250	0.066	0.000	0.000	0.020
1640	1647	0.062	0.012	0.057	0.044
1940	1936	0.054	0.002	0.000	0.035
2240	2246	0.050	0.001	0.000	0.034

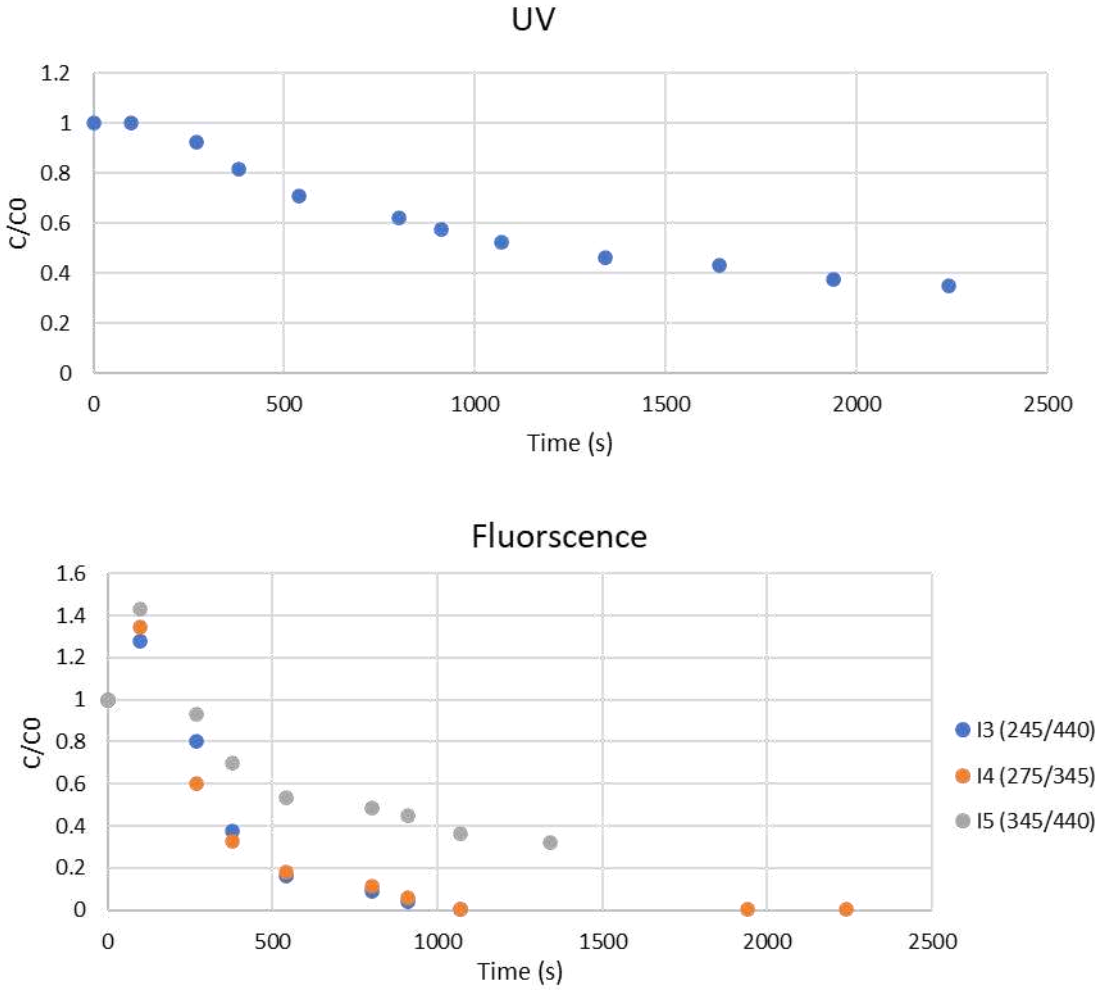

Figure 32: UV (254 nm) and Fluorescence (I3-I4-I5) C/C0 trend in time with UV-LED lamp and 5 mgCl2/l

Linearization and kobs results are showed in Figure 33 and Figure 34. Also with LED lamp better degradation were obtained for I3, with a Kobs of 0.0048.

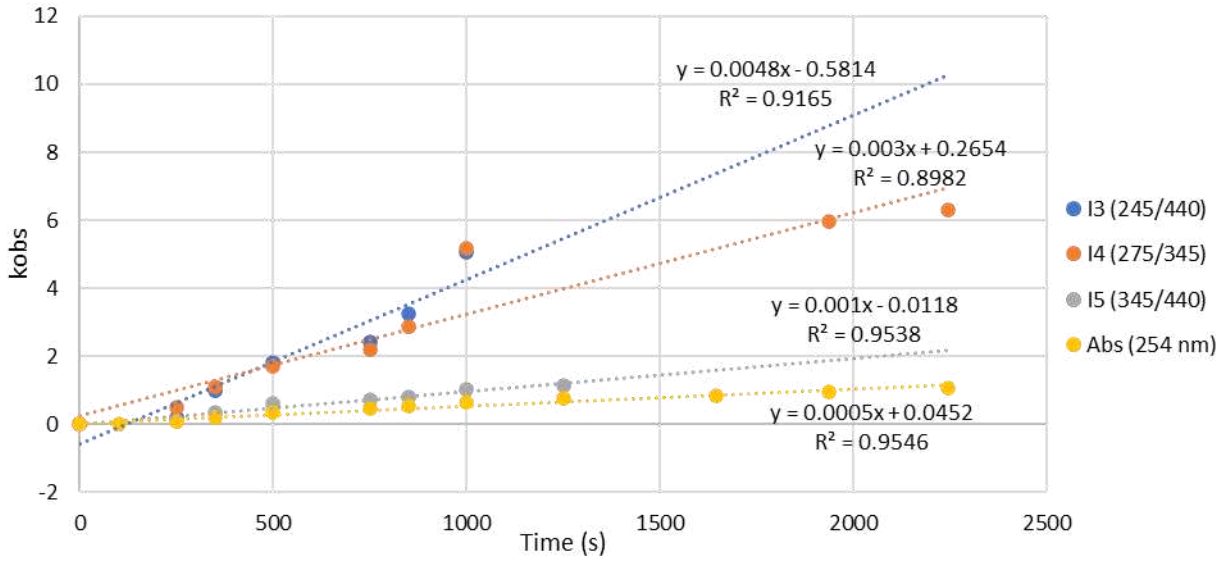

Figure 33: Linearization (test with UV-LED lamp and 5 mgCl2/l)

LED + 5mg/l Cl2	kobs	R2
Abs	0.0005	0.9546
I3	0.0048	0.9165
I4	0.003	0.8982
I5	0.001	0.9538

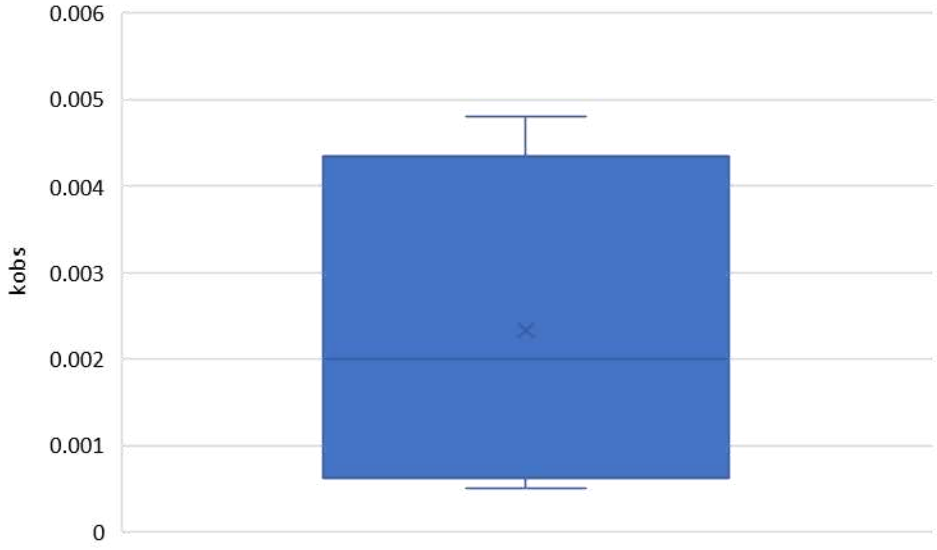

Figure 34¨Kobs and box-plot representation (test with UV-LED lamp and 5 mgCl2/l)

Finally the comparison between the two UV lamp is reported in Figure 35 highlighting that in this case LED lamp showed better results than mercury lamp.

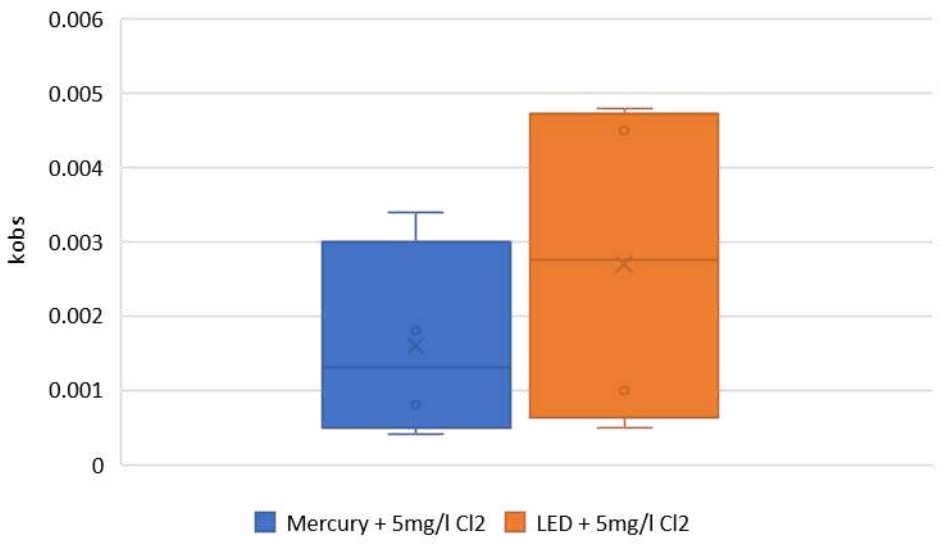

Figure 35: comparison between Mercury and UV-LED lamp with Cl2 as oxidant

5.3 Comparison between H2O2 and Cl2

Finally, a comparison between H2O2 and Cl2 is reported. In Figure 36 for LED and Mercury lamp the box-plot representing the kobs measured with both H2O2 and Cl2 are reported. It is highlighted how LED works more sufficient with Cl2 while having lower performances observed with mercury-H2O2. On the other side, mercury lamp works better with H2O2, but present good performances also with Cl2, even though showing lower than that of the LED lamp.

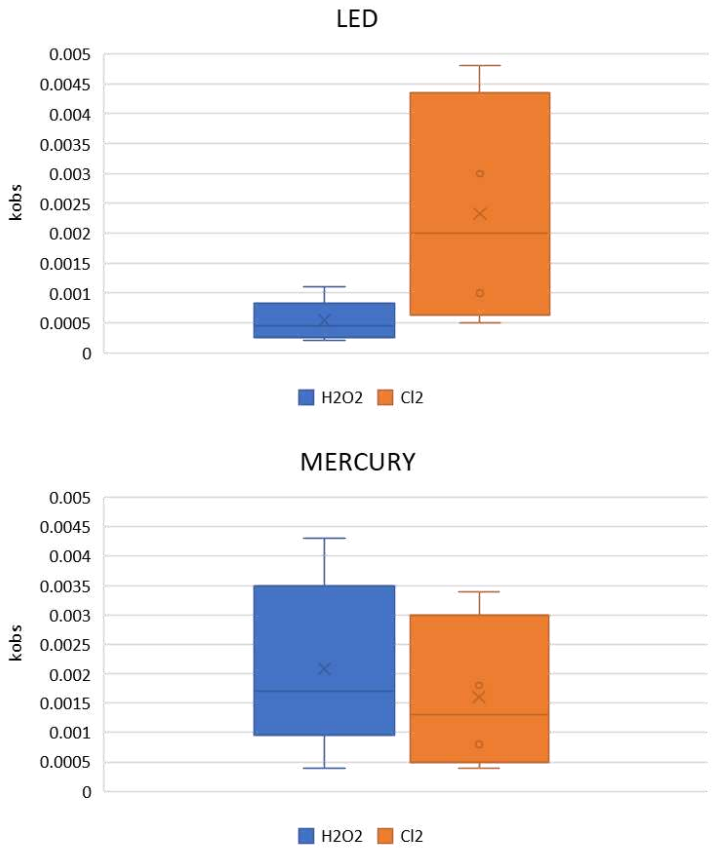

Figure 36: Comparison between Mercury and UV-LED lamp with the two oxidants

5.4 Energy

After having all the results relative to rate constant and their comparison done another aspect of study to be investigated through is to audit the electrical energy consumption that has been used should be discussed, the process determined to provide this electrical energy falls into two category of which electricity kWh has been consumed, the first one is the electrical energy for UV irradiation ($E_{EO,UV}$), and the second category is the equivalent electrical energy for the radical promoter consumption ($E_{EO,RP}$). Also for having a better vision over results the electrical consumption of degradations was once done for the 50% removal and another time for 90% removal of the organics, the results of these electricity consumption is demonstrated all in the following figures for two dosage of H2O2 (30 mg/L, 50 mg/L) and one dosage of Cl2 (5 mg/L).

5.4.1 Results with Mercury lamp

Starting with the test with mercury lamp, at first results regarding the H2O2 dosage of 30 mg/l are reported. In Figure 37 and Table 16 the results illustrate the energy consumption for UV irradiation considering UV absorbance at 254 nm and fluorescence indicators.

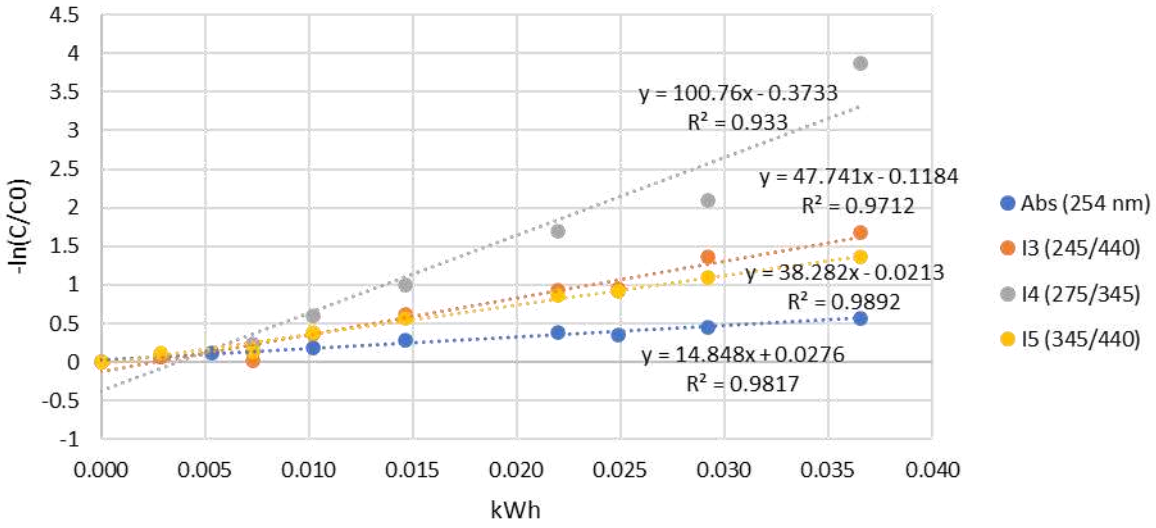

Figure 37: Electrical energy consumption for UV irradiation with Mercury with H2O2 30 mg/L

Table 16: Energy consumption for UV irradiation with Mercury lamp with 30 mgH2O2/l

Mercury + 30 mg/l H2O2	**50% REMOVAL**	**90% REMOVAL**
	kWh	**kWh**
UV	0.045	0.153
I3	0.017	0.051
I4	0.011	0.027
I5	0.019	0.061

Adding the contribution for the oxidant consumption, which was equal to 0.00021 kWh, the final energy consumption was obtained and is reported in Table 17. Highest consumption was obtained for UV which, as reported in the previous section, requires longer time to reach the same removal percentages if compared with fluorescence indices.

Table 17: Total energy consumption for Mercury lamp with 30 mgH2O2/l

Mercury + 30 mg/l H2O2	**50% REMOVAL**	**90% REMOVAL**
	kWh	**kWh**
UV	0.045	0.153
I3	0.017	0.051
I4	0.011	0.027
I5	0.019	0.061

The same elaborations were done also for the dosage of 50 mgH2O2/l. Results regarding the energy consumption for UV irradiation is reported in Figure 38 and Table 18. The consumption associated with the H2O2 dosage was calculated as 0.00035 kWh, and in Table 19 the final energy consumption is reported.

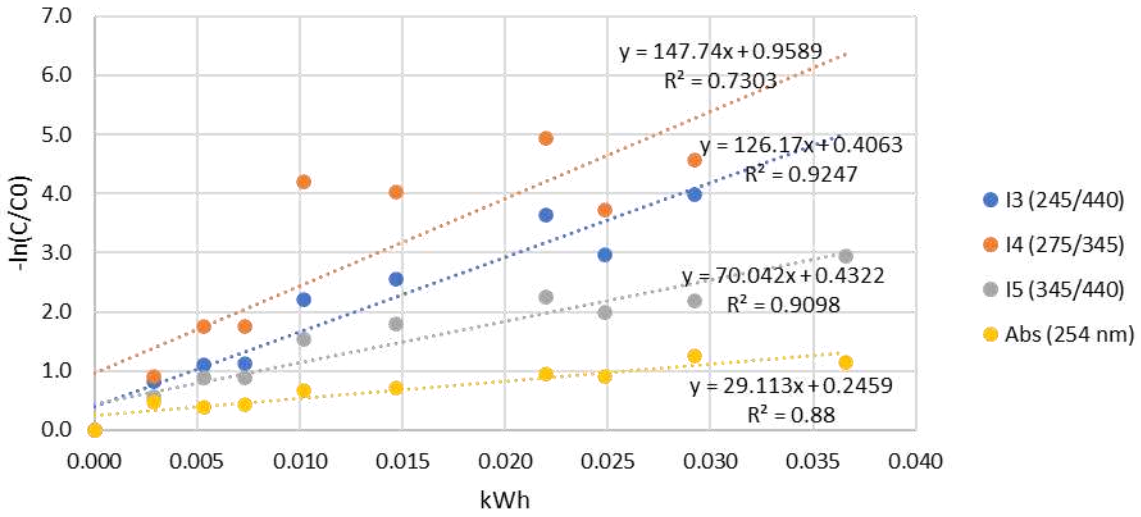

Figure 38: Electrical energy consumption for UV irradiation with Mercury, with H2O2 50 mg/

Table 18: Energy consumption for UV irradiation with Mercury with 50 mgH2O2/l

Mercury + 50 mg/l H2O2	**50% REMOVAL**	**90% REMOVAL**
	kWh	**kWh**
UV	0.015	0.071
I3	0.002	0.015
I4	0.002	0.009
I5	0.004	0.027

Table 19:Total energy consumption for Mercury with 50 mgH2O2/l

Mercury + 50 mg/l H2O2	**50% REMOVAL**	**90% REMOVAL**
	kWh	**kWh**
UV	0.016	0.071
I3	0.003	0.015
I4	0.002	0.009
I5	0.004	0.027

Results for this test showing a lower consumption used comparing to its peer with 30 mg/L which is due to the higher concentration of H2O2 which helped the degradation to speed up.

Finally, results are reported for the mercury lamp adding 5 mg/l of Cl2 as oxidant. Results about the UV irradiation are reported in Figure 39 and Table 20. The consumption connected with the oxidant was calculated as 0.0006 kWh and in the final energy consumption is reported.

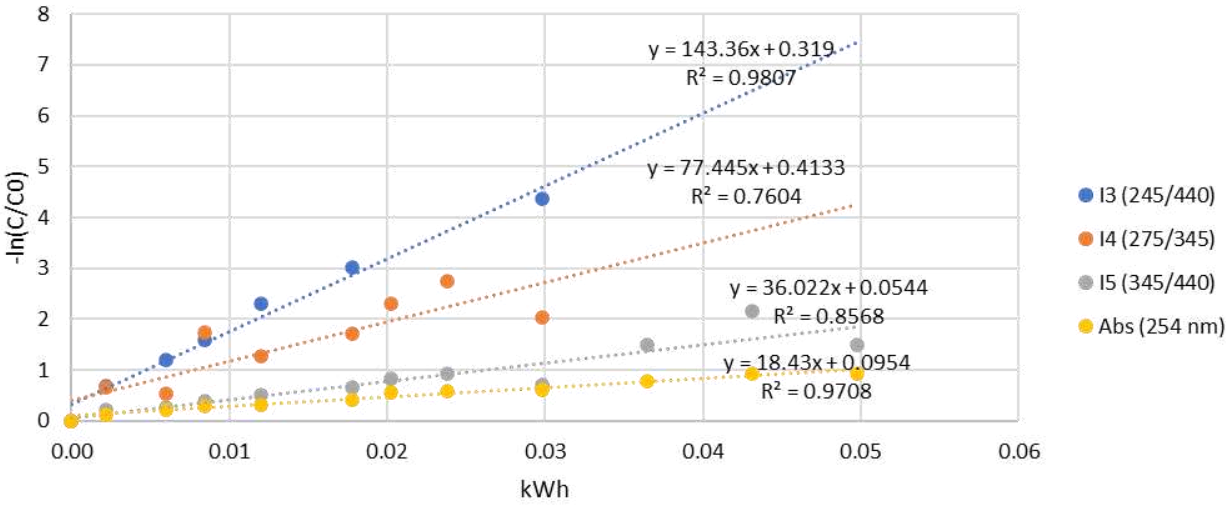

Figure 39: Electrical energy consumption for UV irradiation with Mercury, with Cl2 5 mg/L

Table 20: Energy consumption for UV irradiation with Mercury with 5 mgCl2/l

Mercury + 5 mg/l Cl	**50% REMOVAL**	**90% REMOVAL**
	kWh	**kWh**
UV	0.032	0.120
I3	0.003	0.014
I4	0.004	0.024
I5	0.018	0.062

Table 21: Total energy consumption for Mercury with 5 mgCl2/l

Mercury + 5 mg/l Cl	**50% REMOVAL**	**90% REMOVAL**
	kWh	**kWh**
UV	0.033	0.120
I3	0.003	0.014
I4	0.004	0.025
I5	0.018	0.063

5.4.2 Results with UV-LED lamp

For the Instrument UV-LED with 30 mg/L of H2O2, the results showing the electrical consumption related with UV irradiation is reported in Figure 40 and Table 22.

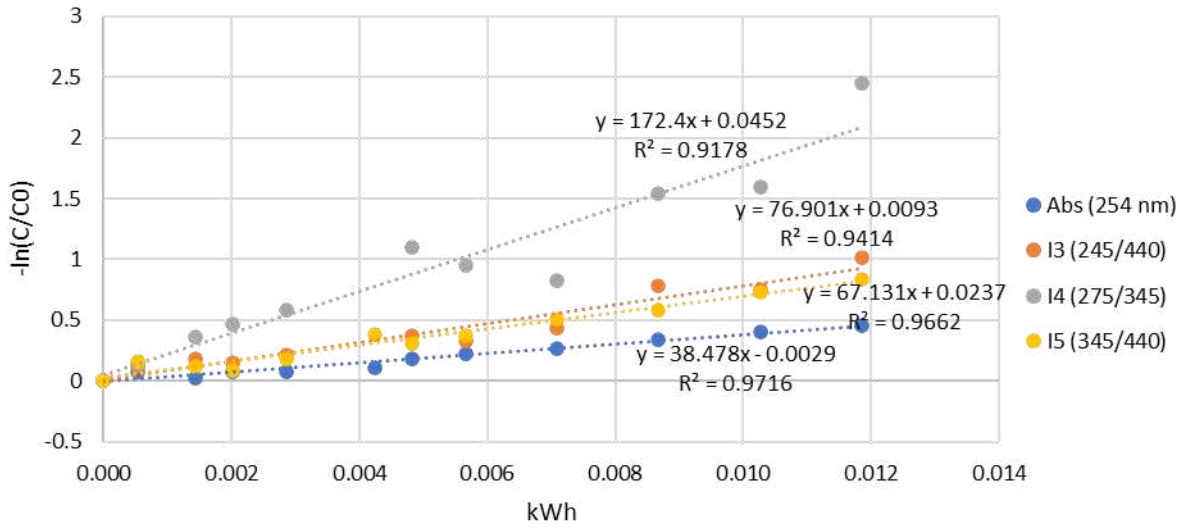

Figure 40: Electrical energy consumption for UV irradiation with UV-LED, with H2O2 30 mg/L

Table 22: Energy consumption for UV irradiation with UV-LED with 30 mgH2O2/l

LED + 30 mg/l H2O2	50% REMOVAL	90% REMOVAL
	kWh	kWh
UV	0.018	0.060
I3	0.009	0.030
I4	0.004	0.013
I5	0.010	0.034

Adding the contribution related with the dosage of the oxidant, which was equal to 0.00021 kWh, the final energy consumption was obtained and is reported in Table 23.

Table 23: Total energy consumption for UV-LED with 30 mgH2O2/l

LED + 30 mg/l H2O2	50% REMOVAL	90% REMOVAL
	kWh	kWh
UV	0.018	0.060
I3	0.009	0.030
I4	0.004	0.013
I5	0.010	0.034

The same elaborations were done also for the dosage of 50 mgH2O2/l. Results regarding the energy consumption for UV irradiation is reported in Figure 41 and Table 24. The consumption associated with the H2O2 dosage was calculated as 0.00035 kWh, and in Table 25 the final energy consumption is reported.

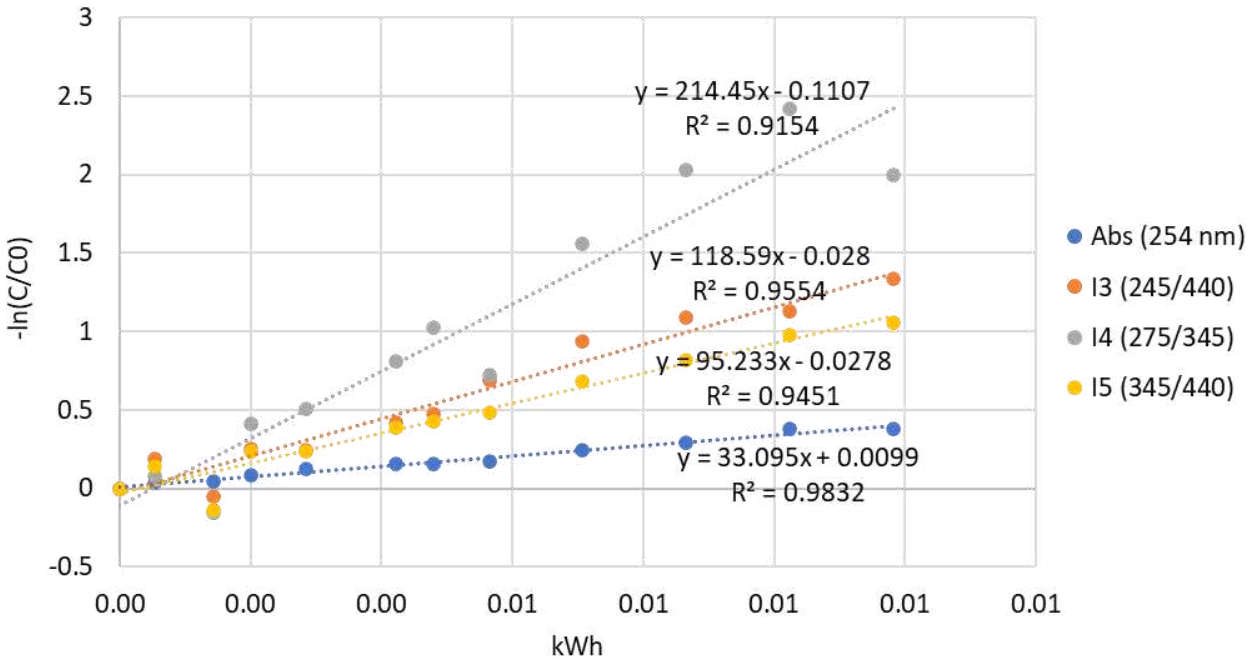

Figure 41: Electrical energy consumption for UV irradiation with UV-LED, with H2O2 50 mg/

Table 24: Energy consumption for UV irradiation with UV-LED with 50 mgH2O2/l

LED + 50 mg/l H2O2	50% REMOVAL	90% REMOVAL
	kWh	kWh
UV	0.021	0.069
I3	0.006	0.020
I4	0.004	0.011
I5	0.008	0.024

Table 25:Total energy consumption for UV-LED with 50 mgH2O2/l

LED + 50 mg/l H2O2	50% REMOVAL	90% REMOVAL
	kWh	kWh
UV	0.021	0.070
I3	0.006	0.020
I4	0.004	0.012
I5	0.008	0.025

In this case there is not a big difference between the two dosages, also because the degradation rate of the two tests were very similar.

Finally, results are reported for the UV-LED lamp with 5 mgCl2/l, in Figure 42 and Table 26 results of energy consumption for UV irradiation are reported. While in Table 27 the total energy consumption is reported considering the consumption connected with Cl2 dosage equal to 0.0006 kWh. Results show lower energy consumption with UV-LED and Cl2 as oxidant if compared with H2O2.

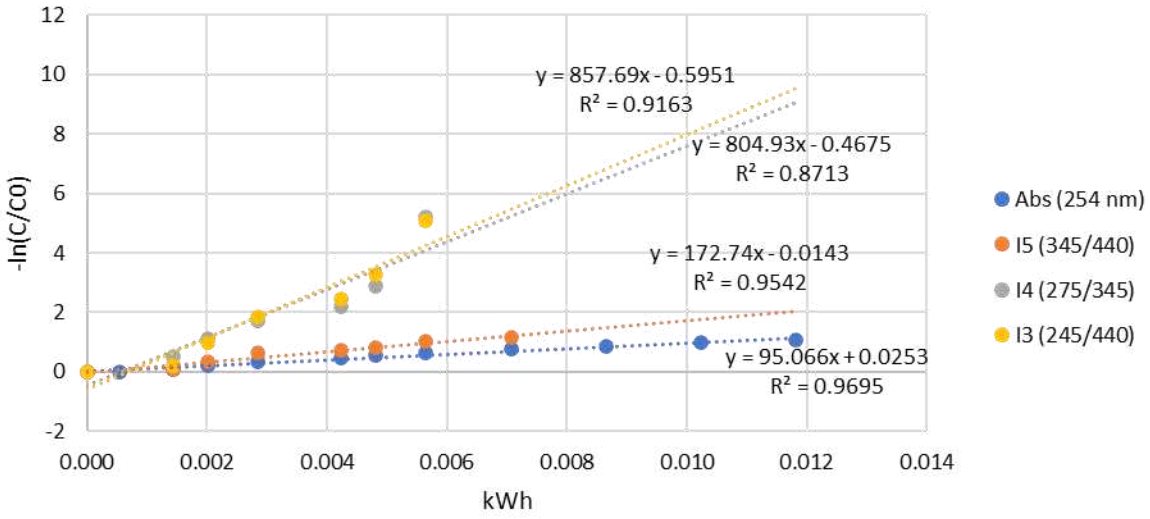

Figure 42: Electrical energy consumption for UV irradiation with UV-LED with Cl2 5 mg/L

Table 26: Energy consumption for UV irradiation with UV-LED with 5 mgCl2/l

LED + 5 mg/l Cl2	50% REMOVAL	90% REMOVAL
	kWh	kWh
UV	0.007	0.024
I3	0.002	0.003
I4	0.001	0.003
I5	0.004	0.013

Table 27:Total energy consumption for UV-LED with 5 mgCl2/l

LED + 5 mg/l Cl2	50% REMOVAL	90% REMOVAL
	kWh	kWh
UV	0.008	0.025
I3	0.002	0.004
I4	0.002	0.004
I5	0.005	0.014

5.4.3 Final comparison

In general, for having an overall comparison among all the tests undertaken it can be concluded that the highest electrical energy consumption is related to the case of Mercury with Cl2 while the lowest amount of energy consumed goes for the case where we used UV-LED instrument with Cl2. UV-LED lamp shows in general lower energy consumption if compared with Mercury lamp.

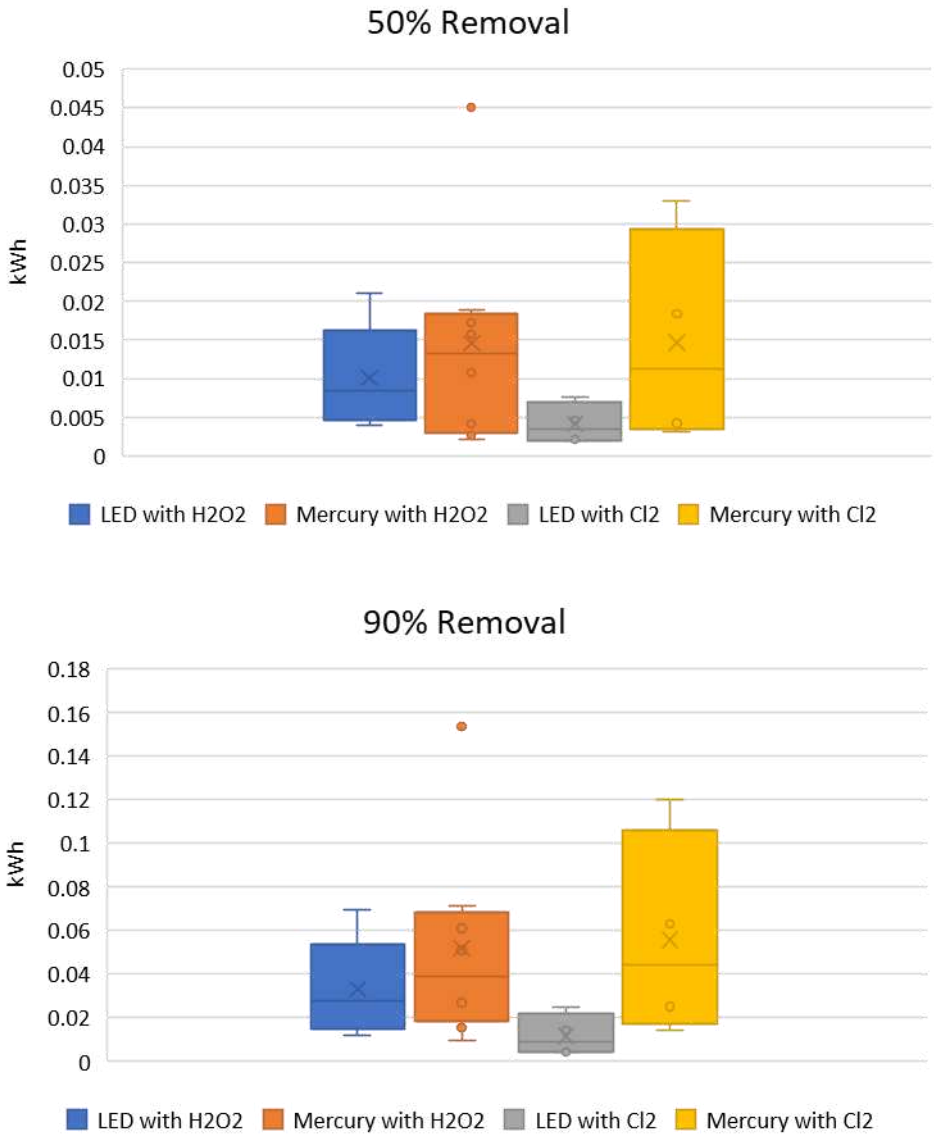

Figure 43: Final comparison of electric consumption at 50% and 90% removal

6. Conclusions

This lab-scale study demonstrates through direct comparison of UV/AOPs in municipal wastewater. The general oxidation performance of a wide range of TOrCs followed the order of UV/H2O2 < UV/Chlorine. In general, there were two different dosage for when the hydrogen peroxide was consumed as to produce radical species [30mg/L and 50mg/L] and one dosage of Chlorine as to produce radicals [5 mg/L] UV/Chlorine exhibited higher compound selectivity than UV/H2O2. For wastewater application, however, other factors like the formation of by-products also need consideration, which was not the focus of this study. Evaluating potential optical surrogates to predict TOrC removal in UV-AOPs, four parameters (fluorescence indices I3(245/440), I4(275/345) and I5(345/440) and UV absorbance at 254nm) were selected representing chromophore and fluorophore features of DOM. Also, in terms of energy consumptions it was noted that the chlorine coupled with the Mercury lamp system showed the highest amount of electrical energy consumption while the lowest amount of energy consumed was regarding the consumption of chlorine coupled with UV-LED lamp. This study showed a significantly useful results to compare the performances of two different UV lamp on spectroscopic parameter. Main results showed that UV-LED lamp is providing better removal rate if coupled with Cl2 (with concentration of 5 mg/L), while mercury showed higher performances when coupled with H2O2 (both concentrations of 30 mg/L and 50 mg/L). Energy consumption seemed to be higher with mercury lamp, in particular when Cl2 was consumed as to produce Radical species. This study was part of a research analysis which could be further implemented by adding other concentrations and other types of oxidants (such as PDS) in order to have a wider range of information and results about the comparison of the two UV lamps.

Bibliography

A. Saravanan, V.C. Deivayanai, P. Senthil Kumar, Gayathri Rangasamy, R.V. Hemavathy, T. Harshana, N. Gayathri, Krishnapandi Alagumalai (2022). A detailed review on advanced oxidation process in treatment of wastewater: Mechanism, challenges and future outlook. Chemosphere, Volume 308, Part 3. https://doi.org/10.1016/j.chemosphere.2022.136524.

Arthur John Allmand, Percy Walmsley Cunliffe and Robert Edwin Witton Maddison, (1925). The photodecomposition of chlorine water and of aqueous hypochlorous acid solutions. Part I. Journal of the Chemical Society Transaction, 127, 822-840. https://doi.org/10.1039/CT9252700822

Autin O., Hart J., Jarvis P., MacAdam J., Parsons S. A. and Jefferson B. (2012). Comparison of UV/H2O2 and UV/TiO2 for the degradation of metaldehyde: kinetics and the impact of background organics. Water Research, 46(17), 5655–5662

Baranda A. B., Fundazuri O. and Martínez de la Maranón I. (2014). Photodegradation of several triazinic and organophosphoric pesticides in water by pulsed light technology. Journal of Photochemistry and Photobiology A: Chemistry, 286, 29–39.

Bolton J.R., Linden K.G. (2003). Standardization of methods for fluence (UV Dose) determination in bench-scale UV experiments. Journal of Environmental Engineering, 129 (3), pp. 209 – 215. 10.1061/(ASCE)0733-9372(2003)129:3(209)

Buxton G. V., Bydder M., Salmon G.A. and Williams J. E. (2000). The reactivity of chlorine atoms in aqueous solution. Part III: the reaction of Cl• with solutes. Physical Chemistry Chemical Physics, 2, 237–245.

Buxton G. V., Greenstock C. L., Helman W. P. and Ross A. B. (1988). Critical review of rate constants for reactions of hydrated electrons, hydrogen atoms and hydroxyl radicals (•OH/•O−) in aqueous solution. Journal of Physical and Chemical Reference Data, 17, 513–886.

Carstea EM, Zakharova YS and Bridgeman J (2018) Online fluorescence monitoring of effluent organic matter in wastewater treatment plants. Journal of Environmental Engineering. 144(5).

Chu and Anastasio at el.(2005) Formation of Hydroxyl Radical from the Photolysis of Frozen Hydrogen Peroxide https://doi.org/10.1021/jp051415f

Crittenden J. C., Trussell R. R., Hand D. W., Howe K. J. and Tchobanoglous G. (2012). Water Treatment: Principles and Design. 3rd edn, John Wiley & Sons Inc., Hoboken, New Jersey, USA

D.B. Miklosa , W.-L. Wangb , K.G. Lindenc , J.E. Drewesa , U. Hübner (2019):Comparison of UV-AOPs (UV/H2O2, UV/PDS and UV/Chlorine) for TOrC removal from municipal wastewater effluent and optical surrogate model evaluation. Chemical Engineering Journal, Volume 362, https://doi.org/10.1016/j.cej.2019.01.041

Dorfman & Adams, at el. (1973), Reactivity of the Hydroxyl Radical in Aqueous Solutions https://doi.org/10.6028/nbs.nsrds.46

Elfrida M. Carstea, John Bridgeman, Andy Baker, Darren M. Reynolds, (2019). Fluorescence spectroscopy for wastewater monitoring: A review. http://dx.doi.org/10.1016/j.watres.2016.03.021

European Commission (2022). Proposal for a DIRECTIVE OF THE EUROPEAN PARLIAMENT AND OF THE COUNCIL Concerning urban wastewater treatment (recast).

G. V. Buxton and M. S. Subhani (1972) Radiation chemistry and photochemistry of oxychlorine ions. Part 2.—Photodecomposition of aqueous solutions of hypochlorite ions https://pubs.rsc.org/en/content/articlelanding/1972/f1/f19726800958

Galina Matafonova, Valeriy Batoev, (2012) Recent progress on application of UV excilamps for degradation of organic pollutants and microbial inactivation, Chemosphere,Volume 89, Issue 6, https://doi.org/10.1016/j.chemosphere.2012.06.012

George V. Buxton and Clive L. Greenstock and W. P. Helman and AlbertaB. Ross, (1988), Critical Review of rate constants for reactions of hydrated electrons, hydrogen atoms and hydroxyl radicals (·OH/·O− in Aqueous Solution

Ghime, D., & Ghosh, P. (2020). Advanced Oxidation Processes: A Powerful Treatment Option for the Removal of Recalcitrant Organic Compounds. Advanced Oxidation Processes - Applications, Trends, and Prospects. doi: 10.5772/intechopen.90192

Goméz-Lopéz V. M. and Bolton J. R. (2016). An approach to standardize methods for fluence determination in benchscale pulsed light experiments. Food and Bioprocess Technology, 9, 1040–1048.

Gregory V. Korshina , Massimiliano Sgroib and Harsha Ratnaweera (2018,) Spectroscopic surrogates for real time monitoring of water quality in wastewater treatment and water reuse https://doi.org/10.1016/j.coesh.2017.11.003

Haag W. R. (1994). Photooxidation of organic compounds in water and air using low-wavelength pulsed xenon lamps. In: Aquatic and Surface Photochemistry, G. R. Helz, R. G. Zepp and D. G. Crosby (eds), Lewis Publishers, Boca Raton, FL, pp. 517–530

INTERNATIONAL UNION OF PURE AND APPLIED CHEMISTRY , FIGURES-OF-MERIT FOR THE TECHNICAL DEVELOPMENT AND APPLICATION OF ADVANCED OXIDATION TECHNOLOGIES FOR BOTH ELECTRIC- AND SOLAR-DRIVEN SYSTEMS (IUPAC) International Union of Pure and Applied Chemistry (iupac.org)

Jennifer G. Pagan and Oliver R. Lawal (2015) , Coming of Age-UVC LED Technology Update https://www.semanticscholar.org/paper/Coming-of-Age-UVC-LED-Technology-Update-Pagan-Lawal/da5db3d09120d99ed2c8116890c6f1952c1c7de0

Liang S., Min J. H., Davis M. K., Green J. F. and Remer D. S. (2003). Use of pulsed-UV processes to destroy NDMA. Journal of the American Water Works Association, 95(9), 121–131.

Lomaev M. I., Sosnin E. A., Tarasenko V. F., Shits D. V., Skakun V. S., Erofeev M. V. and Lisenko A. A. (2006b). Capacitive and barrier discharge excilamps and their applications (Review). Instruments and Experimental Techniques, 49(5), 595–616.

Marshak I. S. (1984). Radiation Characteristics of Flashlamps. Chapter 5 in Pulsed light sources. Consultants Bureau, New York, NY.

Masschelein W. J. (2000). Utilisation des U.V. dans le traiement des eaux. Tribune de l'eau, 53(4–5), 7–107.

Massimiliano Sgroi, Erica Gagliano, Federico G.A. Vagliasindi, Paolo Roccaro, (2020). Absorbance and EEM fluorescence of wastewater: Effects of filters, storage conditions, and chlorination https://doi.org/10.1016/j.chemosphere.2019.125292

Massimiliano Sgroi, Paolo Roccaro, Gregory V. Korshin, et al (2017)Monitoring the Behavior of Emerging Contaminants in WastewaterImpacted Rivers Based on the Use of Fluorescence Excitation Emission Matrixes (EEM)https://pubs.acs.org/doi/10.1021/acs.est.6b05785

Massimiliano Sgroi, Shane A. Snyder, Paolo Roccaro (2021). Comparison of AOPs at pilot scale: Energy costs for micro-pollutants oxidation, disinfection by-products formation and pathogens inactivation. Chemosphere, Volume 273. https://doi.org/10.1016/j.chemosphere.2020.128527.

Massimiliano Sgroi, Tarun Anumol, Federico G.A. Vagliasindi, Shane A. Snyder, Paolo Roccaro, (2021). Comparison of the new Cl2/O3/UV process with different ozone- and UV-based AOPs for wastewater treatment at pilot scale: Removal of pharmaceuticals and changes in fluorescing organic matter. Science of The Total Environment, Volume 765. https://doi.org/10.1016/j.scitotenv.2020.142720.

Metcalf & Eddy, 2014. Wastewater Engineering Treatment and Resource Recovery. Fifth edition, AECOM

Mihaela I. Stefan (2017). Advanced Oxidation Processes for Water Treatment: Fundamentals and Applications. IWA.

N. Mladenov, A. Bigelow, B. Pietruschka, M. Palomo and C. Buckley (2018). Using submersible fluorescence sensors to track the removal of organic matter in decentralized wastewater treatment systems (DEWATS) in real time. Water Science & Technology.

Nowell L. H. and Crosby D. G. (1985). Photodegradation of water pollutants in chlorinated water. In: Water Chlorination: Chemistry, Environmental Impact and Health Effects, R. Jolley W. Davis S. Katz M. Jr, Roberts and V. Jacobs (eds), Lewis Publishers Inc., Chelsea, Michigan, pp. 1055–1062.

Nowell L.H. and Hoigné, J. (1992). Photolysis of aqueous chlorine at sunlight and ultraviolet wavelengths II. Hydroxyl radical production. Water Research, 26(5), 599–605.

Ogata Y. and Tomizawa K. (1984). Photoreaction of benzoic acid with sodium hypochlorite in aqueous alkali. Journal of the Chemical Society, Perkin Transactions 2, 6, 985–988.

Ogata Y., Suzuki T. and Takagi K. (1979). Photolytic oxidation of aliphatic acids by aqueous sodium hypochlorite. Journal Chemical Society, Perkin Transactions 2, 12, 1715–1719.

Oliver B. G. and Carey J. H. (1977). Photochemical production of chlorinated organic in aqueous solutions containing chlorine. Environmental Science & Technology, 11(9), 893–895

Phillips R. (1983). Sources and Applications of Ultraviolet Radiation. Academic Press Inc., New York.

Schaefer R. B., Grapperhaus M., Schaefer I. and Linden K. G. (2007). Pulsed UV lamp performance and comparison with UV mercury lamps. Journal of Environmental Engineering and Science, 6, 303–310.

Schalk S., Adam V., Arnold E., Brieden K., Voronov A. and Witzke H.-D. (2006). UV lamps for disinfection and advanced oxidation: lamp types, technologies, and applications. IUVA News, 8(1), 32–37.

Song K., Mohseni M. and Taghipour F. (2016). Application of ultraviolet light-emitting diodes (UV-LEDs) for water disinfection: a review. Water Research, 94, 341–349

Thomsen C. L., Madsen D., Poulsen J. Aa., Thøgersen J., Knak Jensen S. J. and Keiding S. R. (2001). Femtosecond photolysis of aqueous HOCl. The Journal of Chemical Physics, 115(20), 9361–9369.

Ulrik K. Kläning, Knud Sehested and Thomas Wolff (1984) , Ozone formation in laser flash photolysis of oxoacids and oxoanions of chlorine and bromine https://pubs.rsc.org/en/content/articlelanding/1984/f1/f19848002969

Voronov A., Arnold E. and Roth E. (2003). Long-life technology of high power amalgam lamps. Proceedings of the 2nd International Congress of IUVA, Vienna, Austria, July 9–11